Quantum simulation of non-Abelian lattice gauge theories: A variational approach to $\mathbb{D}_8$ with dynamical matter

Emanuele Gaz,[1] Pavel P. Popov,[2] Guy Pardo,[1] Maciej Lewenstein,[2,3] Philipp Hauke,[4,5] and Erez Zohar[1]

[1]*Racah Institute of Physics, The Hebrew University of Jerusalem, Jerusalem 91904, Givat Ram, Israel*

[2]*ICFO–Institut de Ciencies Fotoniques, The Barcelona Institute of Science and Technology, Av. Carl Friedrich Gauss 3, 08860 Castelldefels (Barcelona), Spain*

[3]*ICREA, Pg. Lluis Companys 23, 08010 Barcelona, Spain*

[4]*Pitaevskii BEC Center and Department of Physics, University of Trento, Via Sommarive 14, I-38123 Trento, Italy*

[5]*INFN-TIFPA, Trento Institute for Fundamental Physics and Applications, Via Sommarive 14, I-38123 Trento, Italy*

(Received 13 March 2025; revised 27 May 2025; accepted 16 June 2025; published 2 July 2025)

Quantum simulation of lattice gauge theories (LGTs) provides a powerful framework for understanding nonperturbative phenomena. However, to realize the hope of answering challenging physics questions on near-term devices it is crucial to develop resource-efficient formulations, in particular for non-Abelian LGTs and beyond (1+1) dimensions. In this work, we address this issue by focusing on the difficulty of simulating fermionic degrees of freedom and on mitigating the Hilbert space redundancy, i.e., the presence of exponentially many nonphysical states that do not obey gauge invariance. First, we show a procedure that removes the matter and improves the hardware-resource efficiency. We demonstrate it for the simplest non-Abelian group addressable with this procedure, $\mathbb{D}_8$, in the cases of both one and two spatial dimensions. Then, with the objective of running a variational quantum simulation on real quantum hardware, we map the $\mathbb{D}_8$ LGT onto qudit systems with local interactions. We propose a variational scheme for the qudit system with a local Hamiltonian, which can be implemented on a universal qudit quantum device. Our results show the effectiveness of the matter-removing procedure, solving the redundancy problem, and reducing the amount of quantum resources. This approach can serve as a way of simulating LGTs in high spatial dimensions, with non-Abelian gauge groups, and including dynamical fermions.

DOI: 10.1103/l8b6-h5s5

I. INTRODUCTION

Gauge theories are fundamental in describing the interactions among the elementary particles in high-energy physics [1]. Their formulation on a discrete spacetime lattice—lattice gauge theories (LGTs)—has become a pivotal tool for the study of fundamental interactions [2,3], particularly in regimes where perturbative methods fail, such as the low-energy dynamics responsible for quark confinement [4]. Traditional approaches to solving LGTs rely on Monte Carlo simulations, which have been widely successful in exploring properties of LGTs [4–6]. However, these methods face significant limitations in addressing real-time dynamics and systems with finite chemical potential, due to the Euclidean time and the sign problem [7]. As such, there has been a growing interest in leveraging new techniques to overcome these challenges.

With the advent of quantum technologies, quantum simulation [8] has emerged as a promising alternative for exploring LGTs beyond the capabilities of classical methods [9,10]. By mapping the gauge and matter fields onto controllable degrees of freedom of a quantum device, it becomes possible to simulate real-time dynamics and tackle problems that are intractable using classical algorithms [11]. Quantum simulation thus holds the potential to revolutionize the study of both static and dynamic properties of strongly coupled gauge theories.

Various quantum simulation schemes for LGTs have been proposed (see, e.g., the reviews [10–19]) and demonstrated across different platforms, from atomic systems [20–24] and trapped ions [25–28] to superconducting qubits [29–32]. Yet, in particular in $d > 1$ the complexity of gauge theories (including their local symmetries), the many-body interactions [5], and the need to handle both fermionic and bosonic fields impose stringent requirements on simulation protocols. These factors contribute to limiting the existing experimental demonstrations of LGTs to specific scenarios. Despite all the pioneering advances, simulating LGTs in higher dimensions remains an outstanding challenge [16], especially in the non-Abelian case and in presence of dynamical matter.

In this paper, we present a general procedure for integrating out fermionic fields in non-Abelian LGTs; see Figs. 1(a) and 1(b). This presents a significant step beyond previous schemes developed for Abelian theories [33–36]. The basic idea is that the intrinsic connection due to the gauge symmetry permits

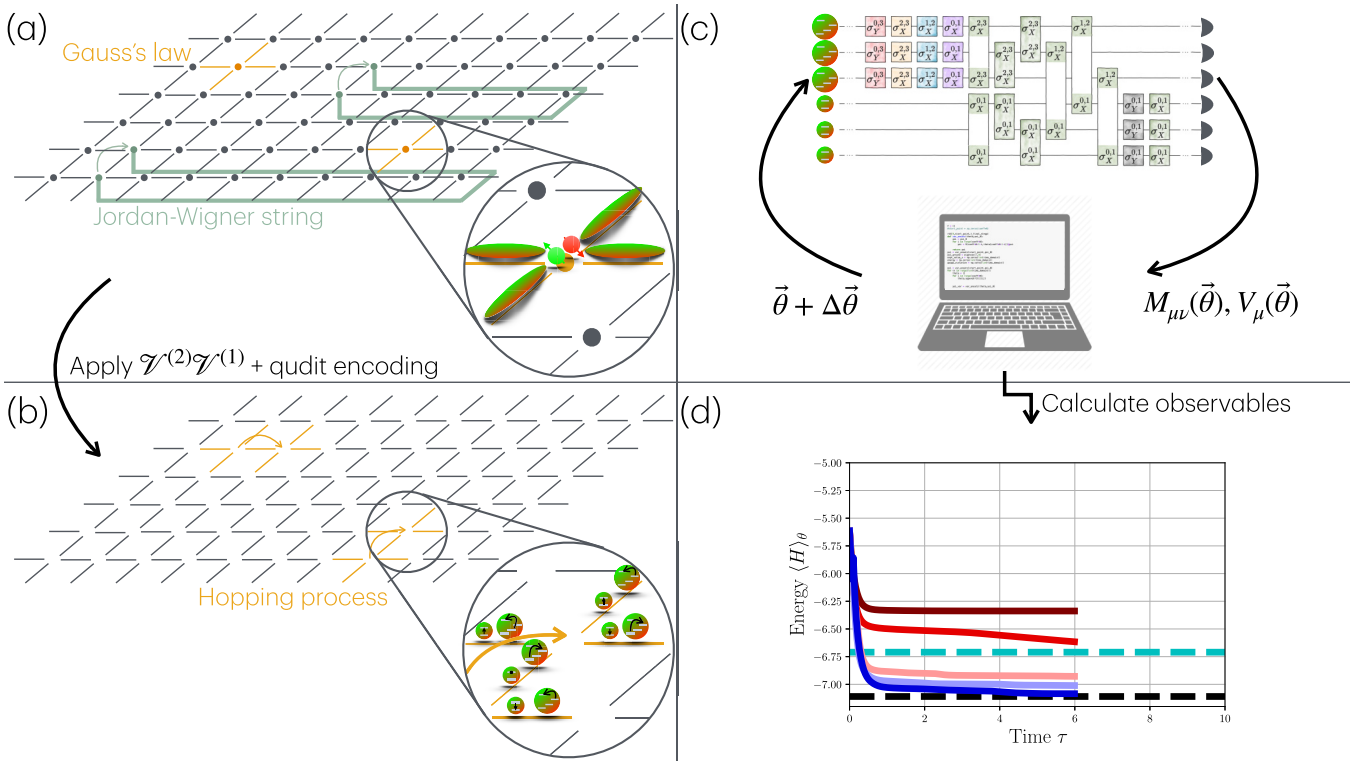

FIG. 1. Quantum simulation of a non-Abelian $\mathbb{D}_8$ lattice gauge theory with dynamical fermionic matter in arbitrary dimensions. (a) In the Kogut-Susskind formulation, dynamical fermions representing the matter are situated on the sites of a lattice and gauge fields reside on the links between the sites. For every vertex (site and the adjacent links), the Gauss's law imposes constraints on the fermionic and gauge field degrees of freedom. Further, to encode the fermionic degrees of freedom on a device capable of quantum computation that does not natively support fermions, one typically introduces nonlocal Jordan-Wigner strings. This approach is not scalable in higher than (1+1) dimensions. (b) In this work, we map the original $\mathbb{D}_8$ LGT onto a qudit quantum hardware by (1) unitarily eliminating the fermionic matter degrees of freedom while keeping the resulting Hamiltonian for the gauge fields local and (2) efficiently encode the gauge field Hilbert space on each link in a qubit and a ququart. This approach is applicable for spatial lattices of arbitrary dimensions. (c) To approximate the ground state of the resulting qudit system, we employ powerful variational optimization techniques for approximating imaginary- and real-time evolution. In a hybrid feedback loop between a quantum and a classical coprocessor, the former allows us to implement a variational quantum circuit and measure quantities relevant for the optimization, whereas the latter serves for solving the corresponding equations of motion and updating the variational parameters. (d) Observables of interest such as the energy of the variational state and others can directly be extracted from the quantum hardware at each step of parameter update, allowing one to reproduce time evolution of a non-Abelian LGT in dimensions beyond (1+1) dimensions.

the gauge fields to keep track of the matter fields. The result is a simplified Hamiltonian that implements the fermionic statistics of matter through local interactions of bosonic degrees of freedom. It thus circumvents the need for encoding, e.g., Jordan-Wigner strings [37], and it removes the exponential redundancy in the simulated Hilbert space, thereby reducing the resource overhead required for simulation on quantum hardware. Our procedure is of particular importance for quantum simulation of higher-dimensional lattices, where other proposals fail to provide scalability.

The general scheme works for both finite and compact Lie groups, including U(N). We illustrate it for the non-Abelian $\mathbb{D}_8$ LGT, which is recently moving into the focus of quantum simulation proposals [38–41], after a significant progress has been made in various different approaches for other finite groups [9,32,35,36,42–58]. We show how the resulting theory can be mapped onto a local Hamiltonian acting on two- and four-level systems locally representing the eight-dimensional Hilbert space of $\mathbb{D}_8$.

$\mathbb{D}_8$ is a favorable choice to demonstrate the procedure for non-Abelian groups for various reasons. For simplicity, we choose to focus on a finite group, whose Hilbert space is easier to understand as well as to encode on current devices. Larger groups, and certainly Lie groups (which are infinite) require truncation procedures. Therefore, one would like to choose the smallest non-Abelian group (in terms of its order, or number of elements) which allows the use of the procedure of [33,34], which is $\mathbb{D}_8$, as explained in Sec. III A. One may argue that this choice is somewhat peculiar, with the $\mathbb{D}_8$ lattice gauge theory having not been explored yet out of the quantum simulation proposals context. However, since this model has the same center as SU(2), the subgroup Z2, and since the center symmetry is related to confinement, it suggests a potential avenue for studying interesting confinement physics that may yield qualitative insights also for physically relevant systems. Therefore, we expect this model, once implemented on quantum devices, to already teach us a significant lesson on standard-model-like confinement

mechanisms, string-breaking phenomena, and topological effects. In parallel, other quantum simulation methods as well as tensor network studies of this model would support each other as sources for benchmarking and comparison.

We formulate a strategy for quantum simulating of the non-Abelian lattice gauge model by employing a variational quantum simulation protocol on a qudit trapped-ions platform [59]; see also Figs. 1(c) and 1(d). The higher-dimensional qudit Hilbert space allows for a compressed representation of the gauge fields, facilitating the design of a resource-efficient simulation protocol that can be used for both ground-state preparation and time evolution [60]. By numerical simulations, we illustrate the performance of the variational algorithm for the case of ground-state preparation of benchmark cases. We demonstrate the feasibility of our method, highlighting its potential for application to a broad range of problems in high-energy physics and beyond. In contrast to other recent proposals, our study thus formulates a model of a non-Abelian gauge theory that is simulable in the laboratory with existing technology, paving the way for future investigations into the rich physics of gauge theories in previously inaccessible regimes.

Our work also leverages recent progress in building qudit-based quantum computers, which has led to the design of simulation protocols for lattice gauge theories based on multilevel quantum systems. In particular, non-Abelian gauge theories can greatly profit from using qudits, due to the complicated structure of the gauge-field Hilbert space. In Refs. [61,62], quantum simulations of SU(2) respectively SU(3) lattice gauge theories in (1+1) dimensions have been proposed, providing concrete examples of possible implementation strategies for non-Abelian gauge theories with qudits. Despite the novelty of these proposals, their applicability is still restricted to 1D lattice geometries. In Ref. [63], a theoretical fermion-qudit quantum processor has been identified as a natural platform for the simulation of non-Abelian gauge theories in arbitrary spatial dimensions. While this work reports an intriguing new possibility for simulating non-Abelian gauge fields beyond one dimension, engineering challenges still restrict its applicability, as the experimental realization of such a fermion-qudit quantum processor is still to be demonstrated. Simulation protocols for models with non-Abelian gauge symmetry are further important for the realization of non-Abelian anyons, relevant for topological quantum computation [64,65]. In that context, qudits have been envisioned as a natural platform to calculate interesting properties of such anyons [66]. As these examples show, there is a great potential for qudit-based quantum simulation for non-Abelian gauge theories, which in turn calls for viable implementation strategies to harness these possibilities.

This paper is organized as follows. In Sec. II we briefly introduce the mathematical description of the target LGT focusing on non-Abelian $\mathbb{D}_8$ as a pedagogical example case. This theory already shows the two key features our formulation takes care of, the fermionic statistics of the matter and the redundancy of the Hilbert space generated by the extensive number of local constraints. Then in Secs. III A and III B we introduce two unitary steps, $\mathcal{V}^{(1)}$ and $\mathcal{V}^{(2)}$, that allow us to eliminate the matter for $\mathbb{D}_8$ in arbitrary dimensions. In Sec. IV we give an outline of the variational algorithm we use. Here we present specific quantum circuits and discuss how the simulation protocol would be implemented on the quantum device. We proceed to presenting a few numerical demonstrations (Sec. VI) of the variational approach for a pseudo-2D system, defined on the minimal lattice for which 1D methods for matter elimination fail. Finally, in Sec. VII we present our conclusions.

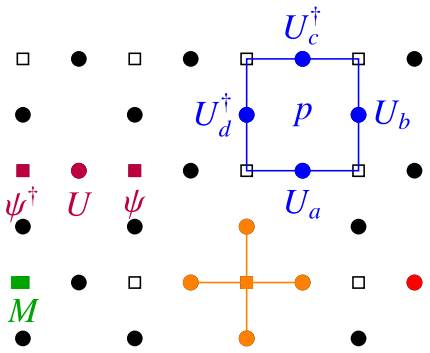

FIG. 2. Illustration of gauge-invariant operators in the $d = 2$ Hamiltonian formulation of LGT. Squares represent matter sites while circles are the gauge fields on the links. The orange cross depicts a local gauge transformation as described in Eq. (19). The red circle is an example of the electric Hamiltonian term we have on all the links; this comes from H_E. The blue plaquette stands for the magnetic Hamiltonian term H_B, and the green square is an example of the local mass term H_M. The purple horizontal line represents a hopping interaction H_{GM}.

II. THE $\mathbb{D}_8$ LATTICE GAUGE THEORY

While lattice gauge theories were first introduced by Wilson in an Euclidean formalism [4], the Hamiltonian formulation of LGTs has emerged as an alternative approach with several distinctive features [5,67]. In the Hamiltonian approach, space is discretized on a d-dimensional lattice $\mathbb{Z}^d$ (square/cubic by default, though formulations in other geometries exist [29]) whereas time remains continuous. This formulation is particularly well suited for real-time dynamics and finite chemical potential problems, both of which are challenging for conventional Monte Carlo methods used in Euclidean lattice field theory [7]. Fermionic matter fields live on the vertices of the lattice, while the links host the gauge fields.

The system has local symmetries generated by the gauge group G, usually a compact Lie or a finite group as in our case considered below ($\mathbb{D}_8$). These *gauge transformations*, $\Theta_g(\mathbf{x})$, are local unitaries under which the physically relevant states and operators are invariant. They are parameterized by group elements $g \in G$ and are associated with the sites $\mathbf{x} \in \mathbb{Z}^d$. The local symmetry introduces conservation laws (*Gauss's law*) on every site. Each $\Theta_g(\mathbf{x})$ acts locally on $\mathbf{x}$ and on the links ℓ around it (starting or ending at $\mathbf{x}$; see Fig. 2), transforming only those degrees of freedom in a way that is parametrized by g. An operator A is gauge invariant if and only if

$$\Theta_g(\mathbf{x}) A \Theta_g^\dagger(\mathbf{x}) = A, \qquad \forall g \in G, \mathbf{x} \in \mathbb{Z}^d, \tag{1}$$

and a gauge-invariant state $|\psi\rangle$ is invariant under all gauge transformations (up to a global phase if G is Abelian; in the

non-Abelian case, gauge transformations can mix the elements of state multiplets [68]).

Despite its advantages, the Hamiltonian formulation of LGTs presents its own challenges. One key difficulty arises from the high dimensionality of the Hilbert space due to the gauge degrees of freedom on each lattice link. Moreover, the need to enforce gauge invariance and the inclusion of dynamical fermions introduces further complexities. It is the purpose of this article to develop an efficient description to circumvent these challenges, by integrating out the matter degrees of freedom and mapping the resulting theory to a qudit Hamiltonian.

A. The group $\mathbb{D}_8$

Although the procedure below is more general, for concreteness we focus on the case $G = \mathbb{D}_8$ (dihedral group of order eight or sometimes known as $\mathbb{D}_4$, the symmetry group of a 4-gon) in two space dimensions. This is the group of planar symmetries of a square, which includes $\pi/2$ rotations and reflections. It is a non-Abelian group, generated by a $\pi/2$ rotation, which we denote by a, and a diagonal reflection about the origin, denoted by y. The dihedral group has recently moved into the attention of quantum simulation proposals [38–41], as its group structure allows for convenient mapping to the discrete degrees of freedom of quantum simulators.

Labelling the identity element by e, we note that

$$a^4 = y^2 = e. \tag{2}$$

Along with

$$yay = a^{-1} \tag{3}$$

one can construct the full multiplication table of the group's eight elements,

$$\begin{aligned}\mathbb{D}_8 &= \{e, a, a^2, a^3, y, ay, a^2y, a^3y\} \\ &= \{a^p y^q | p = 0, 1, 2, 3;\ \ q = 0, 1\}.\end{aligned} \tag{4}$$

The group has five irreducible representations (irreps). Four are 1D unfaithful representations, denoted by $j = 0, \bar{0}, 1, \bar{1}$, representing the group elements as $1, (-1)^q, (-1)^p, (-1)^{p+q}$ respectively. This implies that the 1×1 Wigner matrices for these representations are

$$\begin{aligned} &D^0(a) = 1, \quad D^0(y) = 1, \\ &D^{\bar{0}}(a) = 1, \quad D^{\bar{0}}(y) = -1, \\ &D^1(a) = -1, \quad D^1(y) = 1, \\ &D^{\bar{1}}(a) = -1, \quad D^{\bar{1}}(y) = -1. \end{aligned} \tag{5}$$

The only nontrivial and faithful representation, $j = 2$, may be constructed (for example) out of the generators' Wigner matrices

$$D^2(a) = -i\sigma_y, \quad D^2(y) = \sigma_z. \tag{6}$$

B. The Hilbert space

The matter in our model is fermionic, a crucial feature if one aims for a realistic approximation of models of elementary particles such as electrons, positrons, or quarks. Each site can host two fermionic species of fermions (corresponding to the spinors we have in the nontrivial representation), annihilated by the local Fock operators $\psi_0(\mathbf{x})$ and $\psi_1(\mathbf{x})$,

$$\{\psi_m(\mathbf{x}), \psi_n(\mathbf{y})\} = 0, \quad \{\psi_m(\mathbf{x}), \psi_n^\dagger(\mathbf{y})\} = i\delta_{mn}\delta_{\mathbf{xy}}, \tag{7}$$

where $m, n = 0, 1$ are group indices within the $j = 2$ representation, and $\mathbf{x}, \mathbf{y} \in \mathbb{Z}^2$ are lattice sites. In the following, we assume an implied summation over repeating group indices and, although the discussion can be easily generalized, we focus for concreteness on $d = 2$.

On the links—which we label by $(\mathbf{x} \in \mathbb{Z}^2, i = 1, 2)$, their starting site and the positive direction to which they emanate—the local gauge Hilbert spaces have dimension eight, which equals the group's order. One particular basis of interest is therefore the *group element basis*, $\{|g\rangle\}_{g\in\mathbb{D}_8}$ where elements are identified with each of the elements of the group. Having the two generators a, y, we can represent the elements of this basis in a simpler way, using two quantum numbers, $p = 0, 1, 2, 3$ and $q = 0, 1$:

$$|g\rangle = |a^p y^q\rangle = |p, q\rangle\,. \tag{8}$$

This can be represented exactly by a product of qubit and qudit spaces: the q quantum number will be encoded by the *qubit* and p by a four-level *qudit*, as can be pictorially seen in Fig. 3.

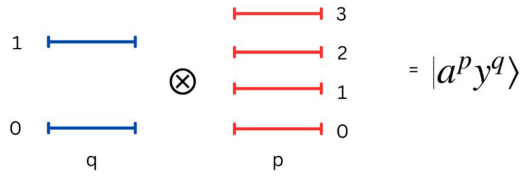

FIG. 3. Decomposition of the link Hilbert space, expressed in the group element basis (8), into a qubit and a qudit.

One can also use the representation basis, whose states $|jmn\rangle$ are labeled by irreps j and eigenvalues of a maximal set of group transformations, m, n. The relation between the groups is through the Peter-Weyl theorem,

$$\langle g|jmn\rangle = \sqrt{\frac{dim(j)}{|G|}} D^j_{mn}(g), \tag{9}$$

using the Wigner matrices $D^j_{mn}(g)$ [69]. In our case, for the nontrivial representation we have the four states $|2mn\rangle$ where $m, n = 0, 1$, and the four states of the unfaithful representations, with no m, n indices (since they correspond to singlets), $|0\rangle\,, |\bar{0}\rangle\,, |1\rangle\,, |\bar{1}\rangle$.

To conclude the link description, we define local unitary operators θ^R_g and θ^L_g acting on the gauge field and transforming it from the right and left sides, respectively. In the group basis, they act as group multiplication operators [70],

$$\theta^R_g\,|h\rangle = |hg^{-1}\rangle \qquad \forall\, h, g \in G, \tag{10}$$

$$\theta^L_g\,|h\rangle = |g^{-1}h\rangle \qquad \forall\, h, g \in G, \tag{11}$$

$$\theta^R_g\,|jmn\rangle = |jmn'\rangle\, D^j_{n'n}(g), \tag{12}$$

$$\theta^L_g\,|jmn\rangle = D^j_{mm'}(g)\,|jm'n\rangle\,. \tag{13}$$

We further introduce the group element operators, U^j_{mn}, which will later be used as the *gauge connections*. They are diagonal in the group element basis, satisfying

$$U^j_{mn}\,|g\rangle = D^j_{mn}(g)\,|g\rangle \tag{14}$$

for every irrep j.

The possible gauge transformations are given by

$$\Theta_g(\mathbf{x}) = W_g(\mathbf{x})\theta^\dagger_{g,\mathrm{M}}(\mathbf{x}) \qquad \forall g \in \mathbb{D}_8, \tag{15}$$

by which the links and matter sites are transformed as

$$W_g(\mathbf{x}) = \prod_{i=1,2}\left[\theta^L_g(\mathbf{x}, i)\theta^{R\dagger}_g(\mathbf{x}-\hat{\mathbf{e}}_i, i)\right], \tag{16}$$

$$\theta^\dagger_{g,\mathrm{M}}(\mathbf{x}) = \det(g^{-1})^{x_1+x_2} e^{-\psi^\dagger_a q_{mn}(g)\psi_b}, \tag{17}$$

$$q(g) = -i\log[D^2(g)]. \tag{18}$$

The latter is related to the staggered fermions [71] prescription for finite gauge groups, as discussed in Ref. [70]. In the above, $W_g(\mathbf{x})$ is a product of operators acting on the links i that are connected to the site $\mathbf{x}$ while $\theta^\dagger_{g,\mathrm{M}}$ acts only on the matter. The differentiation between left (L) and right (R) operators is necessary as $\mathbb{D}_8$ is non-Abelian. $\hat{\mathbf{e}}_i$ are unit vectors in the $i = 1, 2$ directions, As we mentioned before, gauge-invariant states $|\psi\rangle$ satisfy the local *Gauss's law* constraints, which for $\mathbb{D}_8$, assuming no static background charges, can be written in a compact form as

$$W_g(\mathbf{x})\theta^\dagger_{g,\mathrm{M}}|\psi\rangle = |\psi\rangle \quad \forall \mathbf{x} \in \mathbb{Z}^2, \forall g \in \mathbb{D}_8. \tag{19}$$

This is a manifestation of the redundancy of the Hilbert space, in the sense that physical states must obey a number of constraints which is linear with the lattice size. Therefore the physical Hilbert space of gauge-invariant states is exponentially smaller than the full Hilbert space.

C. The Hamiltonian

The Hamiltonian (see Fig. 2) governing the dynamics of the $\mathbb{D}_8$ LGT with dynamical fermions has the form

$$H = H_\mathrm{M} + H_\mathrm{E} + H_\mathrm{B} + H_\mathrm{GM}. \tag{20}$$

For the mass term, H_M, we choose to consider the *staggered* formulation [71]. Moreover, in the representation basis, H_E is given by the number of excitations of the gauge field ($j = 2$); $n_{\mathbf{x},m} = \psi^\dagger_{\mathbf{x},m}\psi_{\mathbf{x},m}$, $m = 0, 1$ (no summation) are the number operators. Explicitly, the different terms of H are

$$H_\mathrm{M} = M\sum_{\mathbf{x}}(-1)^{x_1+x_2}\psi^\dagger_m(\mathbf{x})\psi_m(\mathbf{x}), \tag{21}$$

$$H_\mathrm{GM} = \epsilon\sum_{\mathbf{x},l=1,2}\psi^\dagger_m(\mathbf{x})U_{\mathrm{mn}}(\mathbf{x}, l)\psi_m(\mathbf{x}+\hat{\mathbf{e}}_l) + \mathrm{H.c.}, \tag{22}$$

$$H_\mathrm{B} = \lambda_B\sum_p \mathrm{Tr}[U_a U_b U^\dagger_c U^\dagger_d], \tag{23}$$

$$H_\mathrm{E} = \lambda_E\sum_{\mathrm{links}}|2, mn\rangle\langle 2, mn|\,. \tag{24}$$

In the above, H_E, H_B are the electric and magnetic pure gauge parts, respectively, constituting the Kogut-Susskind Hamiltonian [5] and H_{GM} is the coupling of the gauge fields to the matter [5]. The plaquette convention of H_B is given in Fig. 2.

While in general LGTs the plaquette term as given in H_B is not Hermitian and requires an addition of the Hermitian conjugate; here it is Hermitian as it is. The form of H_E for a finite group may be derived using transfer matrix techniques, as in Ref. [40].

D. Mapping to the qubit-qudit spaces

To implement a quantum simulation on a qudit platform [59], we need to express the operators involved in the Hamiltonian in terms of gates. If possible, we should map the operators into gates that are easy to implement. Knowing the algebra [Eqs. (10) and (11)], we can write down the matrix formulation in the group element basis (8) and conclude that θ_{a^2y}, θ_y, and θ_{a^2} can be easily translated into a qubit and qudit formulation. Defining $\theta_{a^2y} = \theta_0$, $\theta_y = \theta_1$, and $\theta_{a^2} = \Pi$ to simplify notation, a possbile mapping to qubit and qudit operators is

$$\begin{aligned}
\theta^L_{a^2y} &= \theta^L_0 = X\otimes(X_{02}+P_{13}),\\
\theta^R_{a^2y} &= \theta^R_0 = X\otimes(X_{02}+X_{13}),\\
\theta^L_y &= \theta^L_1 = X\otimes(P_{02}+X_{13}),\\
\theta^R_y &= \theta^R_1 = X\otimes\mathbf{1},\\
\theta^L_{a^2} &= \theta^R_{a^2} = \Pi = \mathbf{1}\otimes(X_{02}+X_{13}).
\end{aligned} \tag{25}$$

In this notation, the first operator acts on the qubit space, while the second operates on the qudit. The operator $Z_{\alpha\beta}$ represents a Pauli-Z operator between the α and β levels of the qudit. Similarly, the Pauli-X operator is denoted by $X_{\alpha\beta}$, and the projector into the subspace spanned by the levels α and β is given by $P_{\alpha\beta}$. Henceforth, we shall refer to these as the *generalized Pauli gates*. Whenever there are no level indices it is implied that there are only two levels.

The same mapping to qubit and qudit operators can be done for the connection operators,

$$\begin{aligned}
U_{00} &= \mathbf{1}\otimes Z_{02},\\
U_{01} &= -Z\otimes Z_{13},\\
U_{10} &= \mathbf{1}\otimes Z_{13},\\
U_{11} &= Z\otimes Z_{02}.
\end{aligned} \tag{26}$$

In Appendix A, we explain that these are the only operators present in the transformed Hamiltonian after integrating out the fermionic matter.

III. ELIMINATION OF MATTER

The transformations we now describe enable physics simulation on platforms that do not naturally support fermionic degrees of freedom (e.g., trapped ions or superconducting circuits). In this way, we expand the potential available hardware for quantum simulating LGTs with dynamical matter beyond ultra-cold atomic systems, the original candidates [10].

This transformation has a second advantage. The dynamics of LGTs is highly constrained due to the local symmetries on every site. As a result, out of the full Hilbert space of matter and gauge fields, only an exponentially small part is physical and needs to be simulated. The remainder is redundant, and

often additional overhead is required in order to avoid leakage out of the physical subspace [41]. We resolve this redundancy by integrating out the matter, which significantly decreases the overhead for implementation on the quantum hardware. The final result will be a simplified problem where we deal only with gauge degrees of freedom without losing the properties of fermionic statistics.

A. Bosonic reformulation of the matter

We can replace the fermionic matter of almost any LGT, with only one significant restriction: The construction of the reformulation relies on the existence of a group element whose nontrivial representation is $-\mathbf{1}$ [33]. Thus we can only choose gauge groups that have such an element, or equivalently, groups that include $\mathbb{Z}_2$ as a normal subgroup. This includes both finite and compact Lie groups, such as U(N) for all N and SU(N) for even N. For concreteness, we apply this to the smallest possible non-Abelian group that obeys this condition: While $\mathbb{D}_6$ is the smallest non-Abelian group, it does not contain a $-\mathbf{1}$ element, and thus we opt for $\mathbb{D}_8$.

In this procedure, one applies a unitary and local transformation $\mathcal{V}^{(1)}$ to a product of a state of the original LGT, $|\psi\rangle$, and trivial states of some auxiliary degrees of freedom (which can be disregarded at the end) and employs local, stringless Jordan-Wigner transformations. The result is a state $|\psi^{(1)}\rangle$ where the matter is hard-core bosonic instead of fermionic, and the interaction ranges, while slightly extended, are still local [33]. This is possible due to the local symmetry and in particular its $\mathbb{Z}_2$ central subgroup, which allows one to absorb the statistics by the gauge fields, instead of by the matter.

The hardcore bosonic matter is annihilated by the operators $\eta_m(\mathbf{x})$, with $m = 0, 1$ referring to the two species of matter. Hardcore bosonic operators on different sites commute,

$$[\eta_m(\mathbf{x}), \eta_n(\mathbf{y})] = [\eta_m(\mathbf{x}), \eta_n^\dagger(\mathbf{y})] = 0, \quad \forall \mathbf{x} \neq \mathbf{y}, \tag{27}$$

but anticommute on-site,

$$\{\eta_m(\mathbf{x}), \eta_n(\mathbf{x})\} = 0, \quad \{\eta_m(\mathbf{x}), \eta_n^\dagger(\mathbf{x})\} = \delta_{mn}. \tag{28}$$

The Hamiltonian is transformed according to $\mathcal{V}^{(1)}$, and while the electric part is left unchanged, the other parts obtain the form

$$\begin{aligned} H_{\mathrm{M}}^{(1)} &= M \sum_{\mathbf{x}} (-1)^{x_1+x_2} \eta_m^\dagger(\mathbf{x}) \eta_m(\mathbf{x}), \\ H_{\mathrm{B}}^{(1)} &= \lambda_B \sum_p \xi_p Tr[U_a U_b U_c^\dagger U_d^\dagger], \\ H_{\mathrm{GM}}^{(1)} &= -i\epsilon \sum_{\mathbf{x},l=1,2} \xi_l(\mathbf{x}) \eta_m^\dagger(\mathbf{x}) U_{mn}(\mathbf{x}, l) \eta_m(\mathbf{x} + \hat{\mathbf{e}}_l) + \mathrm{H.c.} \end{aligned} \tag{29}$$

Here the statistics is taken care of by the (operatorial) phase factors [70]

$$\begin{aligned} \xi_h(\mathbf{x}) &= \Pi_v(x) \Pi_h(\mathbf{x} - \mathbf{e_1}) \Pi_v(\mathbf{x} - \mathbf{e_2}) \Pi_v(\mathbf{x} + \mathbf{e_1} - \mathbf{e_2}), \\ \xi_v(\mathbf{x}) &= \Pi_h(\mathbf{x} - \mathbf{e_1}) \Pi_v(\mathbf{x} - \mathbf{e_2}), \\ \xi_p &= \Pi_h(\mathbf{x}) \Pi_v(\mathbf{x} + \mathbf{e_1}) \Pi_v(\mathbf{x} + \mathbf{e_2}) \Pi_h(\mathbf{x} - \mathbf{e_1} + \mathbf{e_2}), \end{aligned} \tag{30}$$

where the h, v subscripts refer to links emanating from the respective sites horizontally and vertically, respectively.

In the Gauss's laws (19), the fermionic operators are simply replaced by the hard-core bosonic ones.

B. Matter removal

To reduce the required amount of quantum resources, and to circumvent the redundancy problem mentioned above, one approach is to eliminate the gauge fields by fully integrating them out. However, this is feasible only in the 1D case (see, e.g., [25,72–74]). In higher dimensions, this procedure is not achievable, but an alternative strategy is to eliminate the bosonic matter instead. In Ref. [34], an elimination scheme for the matter in U(N) and SU(N) theories was proposed. The main idea is to build a unitary transformation, $\mathcal{V}^{(2)}$, which will decouple the matter degrees of freedom from the gauge fields, leaving us with a product of a gauge field state containing all the information, and a trivial matter state that can be disregarded.

Here we proceed to a complete elimination of the matter for a $\mathbb{D}_8$ LGT. In this case, on each site, we have eight Gauss's laws, or constraints, corresponding to the eight group elements; however, only two are necessary to eliminate the two species of matter we have. From the explicit form [Eq. (19)], we observe that the laws associated with the a^2y and y elements result in two independent Gauss's laws, corresponding to two commuting transformations. These provide us with separate, independent constraints for each matter component:

$$W_y(\mathbf{x}) |\psi^{(1)}\rangle = \varepsilon(\mathbf{x}) \big(1 - 2n_1(\mathbf{x})\big) |\psi^{(1)}\rangle, \tag{31}$$

$$W_{a^2y}(\mathbf{x}) |\psi^{(1)}\rangle = \varepsilon(\mathbf{x}) (1 - 2n_0(\mathbf{x})) |\psi^{(1)}\rangle, \tag{32}$$

where, for notation simplicity, we define the staggering term as $(-1)^{x_1+x_2} \equiv \varepsilon(\mathbf{x})$; we also use the number operators $n_1(\mathbf{x}) = \eta_1^\dagger(\mathbf{x}) \eta_1(\mathbf{x})$ and $n_1(\mathbf{x}) = \eta_0^\dagger(\mathbf{x}) \eta_0(\mathbf{x})$. Introducing the projectors

$$P_1^\pm(\mathbf{x}) = \tfrac{1}{2}[1 \mp \varepsilon(\mathbf{x}) W_1(\mathbf{x})], \tag{33}$$

$$P_0^\pm(\mathbf{x}) = \tfrac{1}{2}[1 \mp \varepsilon(\mathbf{x}) W_0(\mathbf{x})], \tag{34}$$

the two independent Gauss's laws can be written as

$$P_0^+(\mathbf{x}) |\psi^{(1)}\rangle = n_0(\mathbf{x}) |\psi^{(1)}\rangle \qquad \forall \mathbf{x}, \tag{35}$$

$$P_1^+(\mathbf{x}) |\psi^{(1)}\rangle = n_1(\mathbf{x}) |\psi^{(1)}\rangle \qquad \forall \mathbf{x}. \tag{36}$$

Finally, we apply a local Jordan-Wigner transformation [37] on each site $\mathbf{x}$,

$$\eta_0(\mathbf{x}) \longrightarrow \tau_0^+(\mathbf{x}), \quad \eta_1(\mathbf{x}) \longrightarrow -\tau_0^z(\mathbf{x}) \tau_1^+(\mathbf{x}), \tag{37}$$

where the τ are Pauli operators. We can then reformulate Eq. (35) and Eq. (36) in a similar form:

$$(P_1^+(\mathbf{x}) - P_1^-(\mathbf{x}))|\psi^{(1)}\rangle = \tau_1^z(\mathbf{x})|\psi^{(1)}\rangle, \tag{38}$$

$$(P_0^+(\mathbf{x}) - P_0^-(\mathbf{x}))|\psi^{(1)}\rangle = \tau_0^z(\mathbf{x})|\psi^{(1)}\rangle. \tag{39}$$

Using these constraints, we can write down a couple of unitaries that locally eliminate the two types of matter

we have

$$\mathcal{V}_1(\mathbf{x}) = P_1^+(\mathbf{x}) \otimes \tau_1^x(\mathbf{x}) + P_1^-(\mathbf{x}) \otimes \mathbf{1}, \tag{40}$$

$$\mathcal{V}_0(\mathbf{x}) = P_0^+(\mathbf{x}) \otimes \tau_0^x(\mathbf{x}) + P_0^-(\mathbf{x}) \otimes \mathbf{1}. \tag{41}$$

The rationale behind this transformation is as follows. If the gauge fields connected to a vertex are projected onto the + subspace, the Gauss's law implies there is a charge at the site, which is removed by the τ^x operator. If they are projected onto −, no charge is present. In both cases, the final charge state is the vacuum.

Since $[\mathcal{V}_n(\mathbf{x}), \mathcal{V}_m(\mathbf{y})] = 0$, we can safely define

$$\mathcal{V}^{(2)} = \prod_{\mathbf{x}} \mathcal{V}_1(\mathbf{x})\mathcal{V}_0(\mathbf{x}). \tag{42}$$

$\mathcal{V}^{(2)}$ is unitary, and it follows that the spectrum of the physical problem does not change even though we have a different Hamiltonian $H^{(2)} = \mathcal{V}^{(2)} H \mathcal{V}^{(2)\dagger}$. We label the transformed states as follows:

$$|\psi^{(2)}\rangle = \mathcal{V}^{(2)}|\psi^{(1)}\rangle. \tag{43}$$

After applying $\mathcal{V}^{(2)}$, the matter at all sites now resides in the ground state [apply $\mathcal{V}^{(2)}$ to Eq. (38)]:

$$\tau_n^z(\mathbf{x})|\psi^{(2)}\rangle = -|\psi^{(2)}\rangle, \quad \forall \mathbf{x}, \quad n = 0, 1. \tag{44}$$

Consequently, the matter spaces can be projected out by working with

$$\tilde{H}^{(2)} = \langle\Omega|H^{(2)}|\Omega\rangle\,, \quad \text{where } |\Omega\rangle = \prod_{\mathbf{x}} |{\downarrow}\rangle_{\mathbf{x},1}\,|{\downarrow}\rangle_{\mathbf{x},0}\,. \tag{45}$$

This procedure (applying $\mathcal{V}^{(2)}$ to $H^{(1)}$ and projecting on $|\Omega\rangle$) is described with more details in Appendix A. Note that H_E, H_M, and H_B are invariant under $\mathcal{V}^{(2)}$. With these transformations, the entire LGT including staggered fermions is encoded into a local Hamiltonian acting only on the gauge degrees of freedom. The simulated Hilbert space has thus been reduced by a factor $4^{\mathcal{N}}$, where $\mathcal{N}$ is the number of vertices (the dimension of the eliminated matter Fock space).

IV. THE VARIATIONAL PROCEDURE

In this section, we discuss the ideas behind the algorithm we propose for quantum simulation of the non-Abelian gauge models under consideration, based on the variational principle. We also outline possible implementation strategies on a specific quantum hardware, trapped-ion qudit quantum computers like the one developed in Ref. [59].

Variational algorithms have emerged as a promising candidate to implement subroutines for resource-efficient quantum simulation [75]. In this approach, a variational ansatz circuit is chosen and efficiently prepared on the quantum device, and a hybrid quantum-classical feedback loop is established. On the quantum device, a set of observables is measured and given as an input to the classical coprocessor. The latter employs a minimization procedure for a preadefined cost function, and calculates the updated parameters of the parametrized nsatz, which are given as input to the quantum device. This procedure is repeated until convergence to an optimal set of parameters is reached. The variational approach can provide an efficient parametrization of many-body states, for example, ground and excited states of a Hamiltonian or even time-evolved states under some unitary evolution. Nevertheless, variational algorithms encounter several difficulties, some of which are due to the current state of quantum technology, while others are more fundamental in nature. Examples of such difficulties are low robustness towards noise [76], overhead in terms of establishing the quantum-classical feedback [77], susceptibility to local minima, and the encounter of barren plateaus [78].

Nevertheless, the variational approach has been applied successfully in numerical simulations in the context of quantum simulation of lattice gauge theories in the past, mostly for systems with Abelian gauge symmetry [51,60,79–86], but also for some non-Abelian toy models [31,87]. In the laboratory, variational protocols have been employed for simulating gauge theory models on a $(1 + 1)$-dimensional [26] and recently on a $(2 + 1)$-dimensional lattice [28]. In the following, we elaborate on the specific variational algorithm used in this work, the variational quantum imaginary time evolution (VarQITE) algorithm [88].

A. The VarQITE algorithm

One can formally write the equation of motion for a quantum state described by a density matrix $\rho(\tau)$ as a function of the (imaginary) time τ as

$$\frac{d}{d\tau}\rho(\tau) = \mathcal{L}[\rho(\tau)]. \tag{46}$$

For a Hamiltonian H, the super-operator reads

$$\mathcal{L}[\rho(\tau)] = -\{H, \rho(\tau)\} + 2\langle H\rangle\rho(\tau), \tag{47}$$

where the average is $\langle\cdot\rangle \equiv \mathrm{Tr}[\rho(\tau)\cdot]$ and the anticommutator $\{A, B\} \equiv AB + BA$. The second term on the right-hand side of Eq. (47) takes care of the normalization of the density matrix, i.e., $\mathrm{Tr}[\rho(\tau)] \equiv 1$.

In the case where we have a parametrized density matrix, $\rho(\tau) = \rho(\boldsymbol{\theta}(\tau))$ for a set of parameters $\boldsymbol{\theta}$, solving Eq. (46) can be cast as a minimization problem; solutions are obtained by minimizing the so-called McLachlan distance,

$$\mathcal{D}(\boldsymbol{\theta}) \equiv \left\| \sum_\mu \frac{\partial\rho}{\partial\theta_\mu}\dot{\theta}_\mu - \mathcal{L}[\rho] \right\|^2, \tag{48}$$

with respect to trajectories of the parameters $\boldsymbol{\theta}(\tau)$. Furthermore, the minimal action principle teaches us that one can formulate equivalent equations of motion for the parameters,

$$\sum_\nu M_{\mu\nu}\dot{\theta}_\nu(\tau) = V_\mu, \tag{49}$$

where the matrix $M_{\mu\nu}$ is the Fubini-Study metric tensor,

$$M_{\mu\nu} = \mathrm{Tr}\left[\frac{\partial\rho}{\partial\theta_\mu}\frac{\partial\rho}{\partial\theta_\nu}\right], \tag{50}$$

and the vector V_μ is defined as

$$V_\mu = \mathrm{Tr}\left[\frac{\partial\rho}{\partial\theta_\mu}\mathcal{L}[\rho]\right]. \tag{51}$$

In this work, we consider a family of trial states given by a parametrized quantum circuit (PQC), as follows:

$$|\psi(\boldsymbol{\theta})\rangle = \mathcal{U}(\boldsymbol{\theta})\,|\psi_0\rangle = U_N(\theta_N)\ldots U_k(\theta_k)\ldots U_1(\theta_1)\,|\psi_0\rangle\,, \tag{52}$$

where $|\psi_0\rangle$ is an initial state and $U_k(\theta_k)$ are unitaries that, acting on the initial state, generate the PQC. With the identification $\rho(\boldsymbol{\theta}) \equiv |\psi(\boldsymbol{\theta})\rangle\langle\psi(\boldsymbol{\theta})|$, one obtains the matrix $M_{\mu\nu}$ and the vector V_μ as follows:

$$M_{\mu\nu} = \mathrm{Re}(\langle\partial_\mu\psi|\partial_\nu\psi\rangle) - \langle\partial_\mu\psi|\psi\rangle\langle\psi|\partial_\nu\psi\rangle \tag{53}$$

and

$$V_\mu = \langle\partial_\mu\psi|H|\psi\rangle + \langle\psi|H|\partial_\mu\psi\rangle = \partial_\mu\langle H\rangle. \tag{54}$$

As long as these quantities depend on the point in the parameter space $\boldsymbol{\theta}$, Eq. (49) is nonlinear and therefore cannot be solved efficiently without resorting to the quantum device. In Ref. [60] one can find a protocol for measuring these quantities on a qudit device. Here we focus on the formulation of the PQC for the ground-state preparation of models with $\mathbb{D}_8$ discrete non-Abelian symmetry.

B. Parametrized quantum circuit for qudits

While the VarQITE algorithm, due to its versatility, holds promise for implementation on various quantum devices based on qubits as well on qudits, in this work we focus on a specific platform—trapped-ion qudit quantum hardware. This makes it possible to define qudit-tailored variational circuits, composed of the gates that are native to the ions. These are single-qubit and qudit (acting on two of the D levels) operations such as X and Y rotations

$$U^{i,j}_{X/Y}(\theta) = \exp\big(-i\theta\sigma^{i,j}_{X/Y}\big) \tag{55}$$

with

$$(\sigma^{i,j}_X)_{m,n} = \begin{cases} 1, & \text{if } (m,n) = (i,j) \text{ or } (j,i) \\ 0, & \text{otherwise} \end{cases} \tag{56}$$

$$(\sigma^{i,j}_Y)_{m,n} = \begin{cases} -i, & \text{if } (m,n) = (i,j) \\ i, & \text{if } (m,n) = (j,i) \\ 0, & \text{otherwise} \end{cases} \tag{57}$$

and entangling qubit and qudit Mølmer-Sørensen (MS) gates

$$\mathrm{MS}^{i,j}_{k,l}(\theta) = \exp\left[-\frac{i\theta}{4}\big(\sigma^{i,j}_X \otimes \mathbf{1} + \mathbf{1}\otimes\sigma^{k,l}_X\big)^2\right]. \tag{58}$$

In Sec. II B we highlighted the fact that our LGT-to-hardware encoding requires a mixed qubit–qudit quantum hardware. This can easily be achieved in the trapped-ion platform because of the possibility to choose two levels in the higher dimensional qudit for information processing. The corresponding two-level rotations then become the Pauli X and Y rotations, and the MS gate acts on the two levels of the qubit.

Specifically, we choose the variational circuit to be of a layered structure, with each layer containing the same type of gates but with a different variational parameter. The specific layers for the circuits used in this work are shown in Figs. 5 and 8. It is worth noting that the single-qudit two-level rotations, combined with the MS entangling gate, constitute a universal set of qudit gates. A subset of these operations, while not necessarily universal, can in practice produce a highly expressive variational ansatz, able to approximate the ground state of the non-Abelian gauge theory models under consideration, as we show below.

We would like to emphasize that our use of the variational method in this work, similarly to the choice of the $\mathbb{D}_8$ gauge group, is done in order to demonstrate and illustrate the resource efficient encoding of the non-Abelian gauge theory. Thus, even though one could make use of the remaining symmetries (e.g., translation, lattice rotation, parity, and charge conjugation invariance) in order to improve the ansatz, we did not do so, and this could be the focus of further study when the same method is applied to specific models of interest.

One should also note that various forms of ansatz states used by us for quantum simulators of non-Abelian lattice gauge theories are quite similar to those use in applications of quantum computing for material science [89] or quantum chemistry [90–92]. In spite of the enormous progress these areas we are still very far from being capable to compete with the best simulations on classical computers [77,93]. Can we reach a quantum advantage with our quantum simulators of lattice gauge theories? Most physicists will say "yes," but the rigorous proof is missing; could it, perhaps, be even too complex to be reached? Nevertheless, we strongly believe that is would be practically impossible to simulate with classical computers dynamics, and even statics of our models given the high expressiveness of the ansatz we use. There are initial publications that try to quantify these issues; hopefully, in the future we will be able to apply these methods to our case.

C. Variational real-time evolution

Before delving into how one can apply the VarQITE algorithm for studying equilibrium properties of non-Abelian gauge theories, we want to briefly discuss the exciting possibility to study out-of-equilibrium physics under non-Abelian symmetry using a slight modification of the VarQITE algorithm. The variational principle can be adapted to real-time evolution [88]: in that case the variational state at each time instance will approximate the time-evolved state under the desired Hamiltonian. For that purpose, Eq. (47) needs to be modified to

$$\mathcal{L}^R[\rho(t)] = -i[H,\rho(t)], \tag{59}$$

so that Eq. (46) becomes the usual Schrödinger equation for the quantum state $\rho(t)$. We denote with t the real time (in contrast to the imaginary time τ) and the superscript R of the super-operator stands for "real." Here we do not need an extra term as in Eq. (47), since the unitary time evolution preserves the trace of the quantum state.

As a consequence, the only modification in the equation of motion for the parameters [Eq. (49)] in case of a parametrized quantum circuit is the right-hand side, which becomes

$$\begin{aligned} V^R_\mu = {} & i(\langle\psi|H|\partial_\mu\psi\rangle - \langle\partial_\mu\psi|H|\psi\rangle) \\ & + i(\langle\partial_\mu\psi|\psi\rangle - \langle\psi|\partial_\mu\psi\rangle)\langle H\rangle. \end{aligned} \tag{60}$$

While this quantity cannot be cast in the form of a gradient of some observable, it is real and therefore can be measured on the quantum device (see [60] for a discussion on specific measuring protocols).

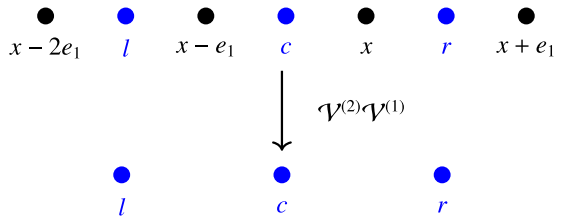

FIG. 4. 1D model, on the top the original model, where the gauge field is represented in blue, and the matter field in black. The lower part shows the transformed model, now featuring only the links, denoted as c, l, and r, corresponding to the center, left, and right, respectively. These labels will be used in subsequent references to indicate the specific link under consideration.

Simulating real-time evolution variationally is certainly an exciting new avenue to be explored. Usually, Trotter formulas provide a controlled approximation to the time-evolution operator, however, the cost of simulating longer times grows linearly in terms of entangling gate count. In the case of a complicated Hamiltonian with several-body terms, implementation of the Trotterization can require unviably many entangling gates even to simulate relatively short-time dynamics. In contrast, the variational real-time evolution procedure can be used to approximate this short-time dynamics using only hardware-friendly resources. For longer-time dynamics, where entanglement is expected to grow significantly and shallow variational circuits are prone to failure, one could still use the variational real-time evolution procedure, combined with a variational Trotter circuit, for more accurate simulations.

V. THE 1D CASE

We begin by analyzing a simple 1D system. This approach allows us to examine the various components of the Hamiltonian, including their representation in terms of gates. We also perform benchmark simulations, whose results align well with theoretical expectations.

A. Theory

The 1D transformed interaction Hamiltonian can be obtained from the general formulation as a special case. As there are no closed loops, in this case we do not have the magnetic (plaquette) term. We use a link-only formulation, where the matter sites are fully eliminated using the procedure given above (see Fig. 4).

In the gate formulation [Eqs. (25) and (26)], the interaction Hamiltonian is given by

$$\tilde{H}_{\mathrm{GM}} = \frac{J}{2}\sum_{\mathbf{x}}\sum_{mn}\hat{H}_{mn}(\mathbf{x}). \tag{61}$$

For each link $\mathbf{x}$, the local interaction term consists of four terms, involving three links—the link $\mathbf{x}$ and its nearest neighbors. To ease to notation, we denote the middle link by c and its neighbors by l and r; see Fig. 4. Then the interaction terms take the form

$$\begin{aligned}
\hat{H}_{00} &= \left(X^l_{02}+X^l_{13}\right)X^cY^c_{02}X^r\left(X^r_{02}+P^r_{13}\right)+X^lX^cY^c_{02},\\
\hat{H}_{01} &= -\left(X^l_{02}+X^l_{13}\right)Z^cY^c_{13}\left(X^r_{02}+X^r_{13}\right)\\
&\quad -X^lZ^cY^c_{13}X^r\left(X^r_{02}+P^r_{13}\right),\\
\hat{H}_{10} &= -Y^c_{13}-X^lY^c_{13}X^r\left(X^r_{02}+P^r_{13}\right),\\
\hat{H}_{11} &= -X^lY^cZ^c_{02}\left(X^r_{02}+X^r_{13}\right)-Y^cZ^c_{02}X^r\left(X^r_{02}+P^r_{13}\right).
\end{aligned} \tag{62}$$

A sum of such terms will give the interaction Hamiltonian for a closed chain. We run our simulation with a chain of four sites and open boundary conditions, hence resulting in only three links for which we can simply keep the l, c, r convention. The middle link will give rise to contributions as above, but we also need to include boundary terms from the transformed contributions of the interaction Hamiltonian on

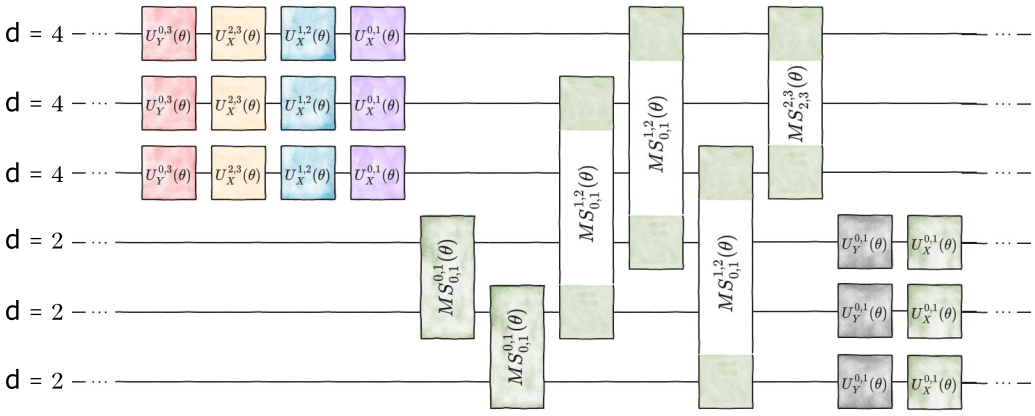

FIG. 5. Individual layer of the parametrized quantum circuit for the 1D system: Each layer of the parametrized quantum circuit used to find the approximate ground state of the 1D system with non-Abelian $\mathbb{D}_8$-symmetry consists of two-level single-qudit rotations on ququarts, entangling two-body MS gates between neighboring qubits, nonlocal MS gates between a qubit and a ququart, and single-qubit Pauli-X and Pauli-Y rotations. Each gate in the variational circuit is parametrized by a variational parameter θ, chosen to be different in each layer. The software used for drawing the quantum circuits is taken from [94]. Note that, in accordance with the convention used in that software, the circuit is to be read from right to left.

the l, r links. For the boundary links (left, L,and right, R) we get

$$\hat{H}^{\mathrm{L}}_{00} = -X^l Y^l_{02} X^c \left(X^c_{02} + P^c_{13}\right) - X^l Y^l_{02}, \tag{63}$$

$$\begin{aligned}
\hat{H}^{\mathrm{L}}_{01} &= -Z^l Y^l_{13}\left(X^c_{02} + X^c_{13}\right) - Z^l Y^l_{13} X^c \left(X^c_{02} + P^c_{13}\right),\\
\hat{H}^{\mathrm{L}}_{10} &= -Y^l_{13} - Y^l_{13} X^c \left(X^c_{02} + P^c_{13}\right),\\
\hat{H}^{\mathrm{L}}_{11} &= +Y^l Z^l_{02}\left(X^c_{02} + X^c_{13}\right) + Y^l Z^l_{02} X^c \left(X^c_{02} + P^c_{13}\right),\\
\hat{H}^{\mathrm{R}}_{00} &= -\left(X^c_{02} + X^c_{13}\right) X^r Y^r_{02} - X^c X^r Y^r_{02},\\
\hat{H}^{\mathrm{R}}_{01} &= -\left(X^c_{02} + X^c_{13}\right) Z^r Y^r_{13} - X^c Z^r Y^r_{13},
\end{aligned} \tag{64}$$

$$\begin{aligned}
\hat{H}^{\mathrm{R}}_{10} &= -Y^r_{13} - X^c Y^r_{13},\\
\hat{H}^{\mathrm{R}}_{11} &= +X^c Y^r Z^r_{02} + Y^r Z^r_{02}.
\end{aligned}$$

The full interaction term is given by

$$\tilde{H}_{\mathrm{GM}} = \frac{J}{2} \sum_{mn} \left(\hat{H}^{\mathrm{L}}_{mn} + \hat{H}_{mn} + \hat{H}^{\mathrm{R}}_{mn}\right). \tag{65}$$

The electric field Hamiltonian and the mass term, in the qubit-qudit scheme, are given by

$$H_{\mathrm{E}} = -\frac{\lambda_E}{2} \sum_{i=l,c,r} \left(X^i_{02} + X^i_{13}\right), \tag{66}$$

$$H_{\mathrm{M}} = -\frac{M}{2} \sum_{i=1,\ldots,4} \hat{H}_{\mathrm{Mi}}, \tag{67}$$

where the i index stands for the different vertices we are considering. The different terms are given by

$$\begin{aligned}
\hat{H}_{\mathrm{M1}} &= X^l \left(X^l_{02} + P^l_{13}\right) + X^l \left(P^l_{02} + X^l_{13}\right),\\
\hat{H}_{\mathrm{M2}} &= X^l \left(X^l_{02} + X^l_{13}\right) X^c \left(X^c_{02} + P^c_{13}\right) + X^l X^c \left(P^c_{02} + X^c_{13}\right),\\
\hat{H}_{\mathrm{M3}} &= X^c \left(X^c_{02} + X^c_{13}\right) X^r \left(X^r_{02} + P^r_{13}\right) + X^c X^r \left(P^r_{02} + X^r_{13}\right),\\
\hat{H}_{\mathrm{M4}} &= X^r + X^r \left(X^r_{02} + P^r_{13}\right).
\end{aligned} \tag{68}$$

Finally, the Hamiltonian we want to simulate for three links is

$$H = H_{\mathrm{E}} + H_{\mathrm{M}} + H_{\mathrm{GM}}, \tag{69}$$

where H_{GM}, H_{E}, H_{M} are given in Eqs. (65), (66), and (67).

B. Simulations

Here we present the numerical results for the variational ground-state preparation of the 1D three-link system. We focus on the likely challenging point of the phase diagram $J = M = h = 1$, where all terms in the Hamiltonian are of a similar energy scale.

The PQC we use in this case is given in Fig. 5. It is composed of single-qudit and single-qubit operations, as well as entangling two-qudit and qubit-qudit operations. The number of entangling operations in each layer is chosen to be $L_{\mathrm{ent}} = L_b + L_d$, where $L_{b/d}$ is the number of qubits and qudits in the system, respectively. Therefore, for a circuit of N layers, the total number of entangling operations that need to be implemented is $L_{\mathrm{ent}} = N(L_b + L_d)$.

We employ the VarQITE algorithm, starting from the initial product state $|\psi_0\rangle = \bigotimes_{i=1}^{3} |1\rangle_{b,i} \otimes |3\rangle_{d,i}$ and initializing the variational parameters of the circuit as $\boldsymbol{\theta} = \mathbf{0}$. The equation of motion with respect to the imaginary time for the variational parameters [Eq. (49)] is solved numerically, producing the trajectories $\boldsymbol{\theta}(\tau)$, which mimic the imaginary time evolution w.r.t. the Hamiltonian H of Eq. (69). In order to take into account the gauge symmetry of the model, we further include a penalty term for the transformed Gauss's law constraint (that is, after the elimination of fermions); for more details we refer to Appendix B 1 c. This is done by adding to the Hamiltonian of the system an extra term $H \to H + \lambda \sum_i G_i^2$, where G_i is the Gauss's law operator at site i and λ is a Lagrange multiplier. As explained in the previous section, the matter elimination procedure does not solve completely the Gauss's law, and therefore, numerically there are still non-gauge-invariant sectors. As it turns out, the ground state manifold of the Hamiltonian without the penalty term has twofold degeneracy: one of the states is the true gauge-invariant vacuum and the other one is outside the gauge-invariant sector. By adding the penalty term with $\lambda > 0$, we lift this degeneracy and allow the VarQITE algorithm to converge to the true (gauge-invariant) ground state. In order to ensure numerical stability, we choose $\lambda = 0.1$, which we find already sufficient for this purpose.

For each time τ and set of parameters $\boldsymbol{\theta}(\tau)$, we calculate the expectation value of the Hamiltonian in the trial state $E(\boldsymbol{\theta}) = \langle\psi(\boldsymbol{\theta})| H |\psi(\boldsymbol{\theta})\rangle$ as well as the fidelity w.r.t. the ground state $|\psi_{\mathrm{ground}}\rangle$ of H obtained by exact diagonalization, defined by

$$\mathcal{F}_\theta(\tau) = |\langle\psi(\theta(\tau))|\psi_{\mathrm{ground}}\rangle|^2. \tag{70}$$

In Figs. 6(a) and 6(b), those two quantities are shown as a function of the imaginary time τ. For a variational circuit, composed of a total number of $N = 3$ layers, the fidelity with respect to the ground state is already as high as 99%. The total number of entangling operations in the circuit with $N = 3$ layers is $L_{\mathrm{ent}} = 3(3 + 3) = 18$.

VI. THE 2D CASE

Above we have analyzed the transformation properties of the Hamiltonian under various transformations [33,34] and provided a simple 1D example. Here we generalize to higher dimensions, where these transformations are really needed, and identify the complexity of the interactions in the Hamiltonian in terms of generalized Pauli gates.

The 2D system involves many-body interactions; for example, the horizontal interaction Hamiltonian contains a five-link and a seven-link interaction. Importantly, in our formulation, each link comprises both a qubit and a qudit, meaning a seven-link interaction could involve more than seven bodies. Table I provides a concise summary of the interactions.

Given these considerations, the terms may involve up to interacting 12 bodies, rendering it impractical to implement this theory with current hardware capabilities, through either a purely analog or digital approach. Alternatively, we can employ a hybrid quantum-classical protocol for quantum simulation—the variational time-evolution algorithm. In this approach, the experimental overhead one is willing to spend can be directly chosen, and the accuracy of the algorithm can

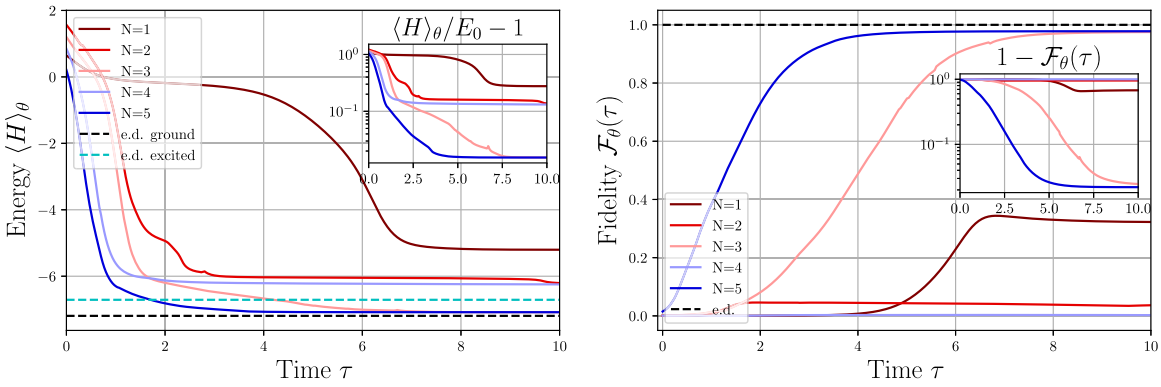

FIG. 6. VarQITE for the 1D system: (a) The energy of the variational state $|\psi(\boldsymbol{\theta})\rangle$ as a function of the imaginary time for $N = 1, 2, 3, 4, 5$ number of layers. The dashed black line shows the numerical value of the true ground state, whereas the cyan line the one of the numerical non-gauge-invariant first excited state (see Sec. V B for a discussion of its origin). After initial fast convergence to low energies, the secondary slow optimization is primarily due to the penalty for Gauss's law violation. From the inset, one can deduce that after $\tau = 5$, the optimization practically stops, yielding a relative error $\sim$1% for $N = 5$ layers. (b) The fidelity of the variational state w.r.t. the true ground state from exact diagonalization as a function of the imaginary time τ. As for the energy, the optimization practically stops after $\tau = 5$, leading to a fidelity of $\sim$99% for $N = 5$ layers.

be estimated accordingly. We verify the resulting Hamiltonian by considering two specific 2D systems that are small enough to be solved using semianalytical methods. This allows us to compare the spectrum of the original theory with that of the matter-eliminated theory within the chosen sector. The details of this verification are in Appendix B.

Next, we present the numerical results for the variational ground-state preparation of a pseudo-2D system, shown in Fig. 7. This model is the simplest nontrivial 2D lattice available to benchmark the matter elimination procedure, in the sense that it is the simplest for which which 1D methods fail [35].

As in Sec. V B, we again focus on the likely challenging point of the phase diagram $J = M = h = 1$, and employ the VarQITE algorithm in order to find an approximation of the ground state. Again, the variational circuit we use is composed of single-qubit, single-qudit, qubit-qudit, and two-qudit gates that can be implemented in the trapped-ion qudit platform natively, ensuring the feasibility of our protocol. In Fig. 8 one layer of the circuit that implements the variational ansatz is shown.

To initialize the VarQITE minimization, we choose the product state $|\psi_0\rangle = \bigotimes_{i=1}^{3} |1\rangle_{b,i} \otimes |3\rangle_{d,i}$ and the variational parameters $\boldsymbol{\theta} = \mathbf{0}$. At every step of the imaginary time evolution, we calculate the energy of the variational state $E(\boldsymbol{\theta}) = \langle\psi(\boldsymbol{\theta})| H |\psi(\boldsymbol{\theta})\rangle$ and the fidelity w.r.t. the exactly diagonalized ground state $|\psi_{\text{ground}}\rangle$ of H. Here, as in the case of the 1D system, we add to the Hamiltonian the penalty term $H \to H + \lambda \sum_i G_i^2$, where G_i is the Gauss's law operator at site i and λ is a Lagrange multiplier. Here, for numerical stability of the VarQITE algorithm, we choose $\lambda = 0.05$.

In Fig. 9(a), the course of minimization of the cost function—the energy—is shown, and in Fig. 9(b) the fidelity with respect to the ground state. A fidelity over 95% is reached already for $N = 3$ layers, whereas for $N = 5$ layers the fidelity is over 99%, corresponding to variational circuits with a total of $L_{\text{ent}} = 3(4 + 4) = 24$ and $L_{\text{ent}} = 5(4 + 4) = 40$ two-body entangling gates, respectively.

In Appendix C we discuss, both qualitatively and quantitatively, the single-plaquette case, the minimal instance in which the plaquette interaction is included.

TABLE I. Features of the various components of the Hamiltonian. By "hardest" we refer to the component involving the highest number of bodies. From an experimental standpoint, the notion of hardness may vary, given that qubits and qudits present differing implementation challenges.

	Max. # bodies	Structure of the "hardest" term
Electric term	1	1 qudit
Magnetic term	10	4 qubits + 6 qudits
Vertical int.	12	7 qubits + 5 qudits
Horizontal int.	11	7 qubits + 4 qudits

VII. DISCUSSION AND SUMMARY

In this work, we have addressed two key challenges in the quantum simulation of lattice gauge theories (LGTs) beyond 1D setups: the simulation of fermionic matter and

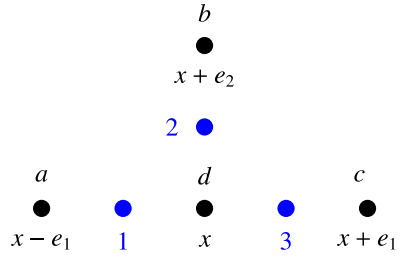

FIG. 7. Pseudo-2D model, in blue the gauge field while in black the matter before being removed. We take a, b, and c as the even sites and d as the odd one. Per each site we have at most two fermions, and they correspond to two different flavours; we are using the fundamental representation for the matter. The numbers will be used subsequently to reference the specific link under consideration.

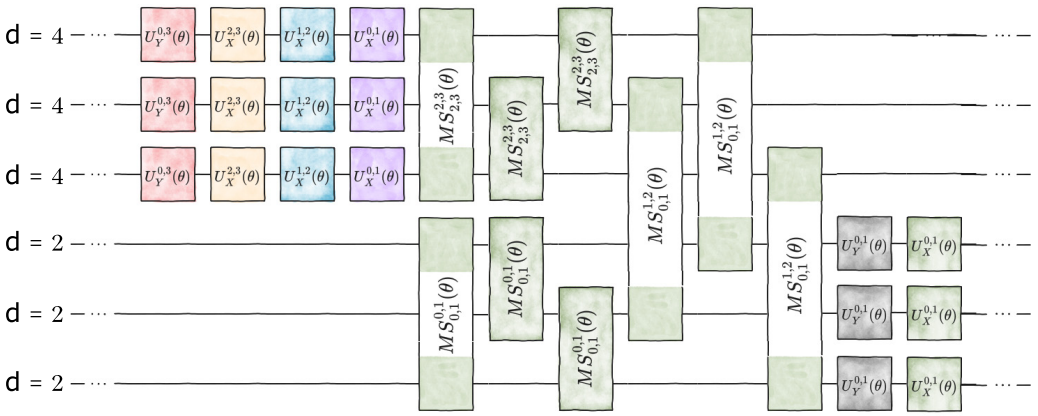

FIG. 8. Individual layer of the parametrized quantum circuit for the pseudo-2D system. Each layer of the parametrized quantum circuit used to find the approximate ground state of the pseudo-2D system with non-Abelian $\mathbb{D}_8$ symmetry consists of two-level single-qudit rotations on the ququarts, entangling two-body MS gates between each pair of qubits and each pair of ququarts, nonlocal MS gates between a qubit and a ququart, and single-qubit Pauli-X and Pauli-Y rotations. Each gate in the variational circuit is parametrized by a variational parameter θ, which differs between different layers. Note that, in accordance with the convention used in the drawing software [94], the circuit is to be read from right to left.

the redundancy in the Hilbert space. We have generalized transformation methods previously employed only in Abelian cases [33,34] to non-Abelian theories. By applying them to the case of a $\mathbb{D}_8$ LGT with staggered fermions, we have demonstrated their effectiveness in simplifying the theory and reducing resource requirements. As we have shown through analytical checks, the spectra of the system remain identical before and after the transformation, evidencing the faithfulness of the mapping. Further, by performing numerical simulations based on the variational principle for a parametrized quantum circuit on a trapped-ion qudit platform, we were able to show that using only an experimentally friendly amount of resources in terms of gate count, the true ground state of 1D and 2D models with a $\mathbb{D}_8$ non-Abelian gauge symmetry can be approximated with high accuracy in an experimentally relevant setup. Increasing the number of layers of alternating single-qudit and two-qudit entangling gates shows rapid improvements, both in terms of the value of the energy and in the fidelity with respect to the exactly diagonalized ground state. The relative error approaches 1% for entangling gate count as low as 18 in the 1D case and 40 in the 2D case. The proposed algorithm can therefore be implemented with available resources on existing quantum hardware, and if it is chosen as a testbench for experimental realizations, computations in other methods (e.g., classical Markov Chain Monte Carlo, or fermionic tensor network methods [95,96]) could be performed in order to allow for proper comparison.

Looking ahead, apart from digital quantum simulations on actual quantum devices, future research could focus on extending the elimination techniques to more complex non-Abelian groups. This, in turn, could allow for the

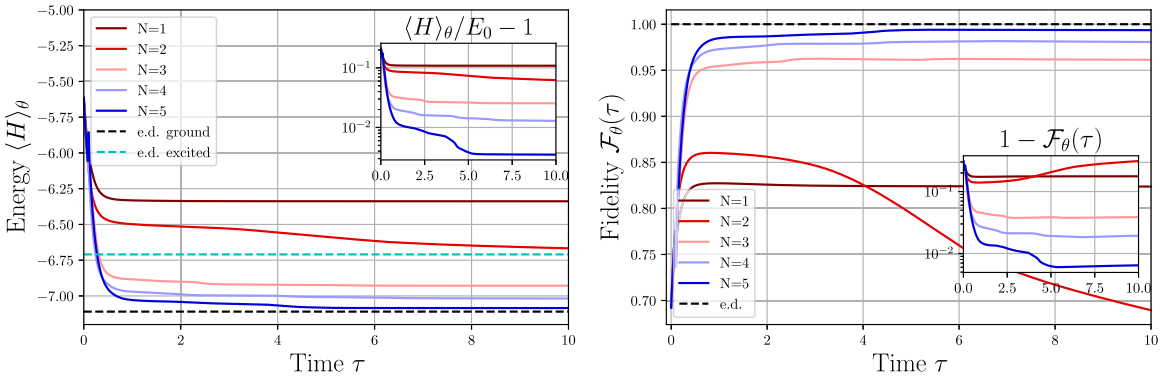

FIG. 9. VarQITE for the pseudo-2D system: (a) The energy of the variational state $|\psi(\boldsymbol{\theta})\rangle$ as a function of the imaginary time for $N = 1, 2, 3, 4, 5$ number of layers. The dashed black line shows the numerical value of the true ground state, whereas the cyan line of the numerical non-gauge-invariant first excited state (see Sec. VI and the discussion in Sec. V B). After initial fast convergence to low energies, the secondary slow optimization is primarily due to the penalty for Gauss's law violation. From the inset, one can deduce that after $\tau = 5$, the optimization practically stops, rendering relative error $<1\%$ for $N = 5$ layers. (b) The fidelity of the variational state w.r.t. the true ground state from exact diagonalization is shown as a function of the imaginary time τ. As for the energy, the optimization practically stops after $\tau = 5$, rendering fidelity w.r.t. the ground state of $>99\%$ for $N = 5$ layers.

exploration of phenomena such as confinement and deconfinement, and potentially offer insights into the physical behavior of lattice gauge theories. Furthermore, the variational principle, although only applied to equilibrium setups here, can be straightforwardly generalized and applied to studying nonequilibrium dynamics of models with non-Abelian gauge symmetry, relevant, for example, for heavy-ion collision experiments and early-universe structure dynamics [97]. From the implementation point of view, there is value in developing new tools that simplify quantum simulations, potentially by reducing degrees of freedom or minimizing required resources. Additionally, exploring methods for simulating compact Lie groups like U(N) or SU(N) may offer new directions for overcoming current experimental and technological limitations in quantum LGT simulations, specifically, because these groups can give interesting insights into both strong and weak interactions. It will also be interesting to test if these methods can simplify numerical calculations of non-Abelian groups in higher dimensions. The matter elimination procedure is well defined for these groups, with the exception that for SU(N) we need N to be even (see [33] and Sec. III A). Then to construct a complete quantum simulation proposal for these groups one would have to encode the gauge field degrees of freedom into some available quantum simulator. This can be achieved using an approximated truncation of the infinite dimensional local Hilbert space (e.g., [98–101]).

ACKNOWLEDGMENTS

E.Z. acknowledges the support of the Israel Science Foundation (Grant No. 374/24). The ICFO-QOT group acknowledges support from the European Research Council AdG NOQIA; MCIN/AEI Grants No. (PGC2018-0910.13039/501100011033, No. CEX2019-000910-S/10.13039/501100011033, Plan National FIDEUA Grants No. PID2019-106901GB-I00, Plan National STAMEENA PID2022-139099NB, I00, project funded by MCIN/AEI/10.13039/501100011033, and the "European Union NextGenerationEU/PRTR" (PRTR-C17.I1), FPI); QUANTERA MAQS PCI2019-111828-2; QUANTERA DYNAMITE Grant No. PCI2022-132919, QuantERA II Programme co-funded by European Union's Horizon 2020 program under Grant Agreement No. 101017733; Ministry for Digital Transformation and of Civil Service of the Spanish Government through the QUANTUM ENIA project call–Quantum Spain project, and the European Union through the Recovery, Transformation and Resilience Plan–NextGenerationEU within the framework of the Digital Spain 2026 Agenda; Fundació Cellex; Fundació Mir-Puig; Generalitat de Catalunya (European Social Fund FEDER and CERCA program, AGAUR Grant No. 2021 SGR 01452, QuantumCAT U16-011424, co-funded by ERDF Operational Program of Catalonia 2014-2020); Barcelona Supercomputing Center MareNostrum (FI-2023-3-0024); funded by the European Union (HORIZON-CL4-2022-QUANTUM-02-SGA PASQuanS2.1, 101113690, EU Horizon 2020 FET-OPEN OPTOlogic, Grant No. 899794, QU-ATTO, 101168628), ICFO Internal "QuantumGaudi" project; European Union's Horizon 2020 program under the Marie Sklodowska-Curie Grant Agreement No. 847648; and "La Caixa" Junior Leaders fellowships, La Caixa" Foundation (ID 100010434): CF/BQ/PR23/11980043.

This project has received funding from the European Union's Horizon Europe research and innovation programme under Grant Agreement No. 101080086 NeQST. P.H. has further received funding from the QuantERA II Programme through the European Union's Horizon 2020 research and innovation program under Grant Agreement No. 101017733, from the European Union under NextGenerationEU, PRIN 2022 Prot. No. 2022ATM8FY (CUP: E53D23002240006), and from the European Union under NextGenerationEU via the ICSC–Centro Nazionale di Ricerca in HPC, Big Data and Quantum Computing. Views and opinions expressed are those of the authors only and do not necessarily reflect those of the European Union or the European Commission. Neither the European Union nor the granting authority can be held responsible for them. This work was supported by Q@TN, the joint laboratory between the University of Trento, FBK—Fondazione Bruno Kessler, INFN—National Institute for Nuclear Physics, and CNR—National Research Council. P.P.P. also acknowledges support from the "Secretaria d'Universitats i Recerca del Departament de Recerca i Universitats de la Generalitat de Catalunya" under Grant No. 2024 FI-3 00390, as well as the European Social Fund Plus.

E.G., P.P.P., and G.P. contributed equally to this work.

DATA AVAILABILITY

The data that support the findings of this article are openly available [102].

APPENDIX A: MATTER REMOVAL TRANSFORMATION

In this appendix, we provide additional information regarding the matter removal process, going from the bosonic reformulation setting to the one without matter at all. This serves as an expanded explanation of the procedure introduced in Sec. III B.

We start by studying how the single elements of the Hamiltonian terms are transformed under $\mathcal{V}^{(2)}$ defined in Eq. (42):

$$\mathcal{V}^{(2)}\tau_n^{\pm}\mathcal{V}^{(2)\dagger} = P_n^{+}\tau_n^{\mp} + P_n^{-}\tau_n^{\pm}, \tag{A1}$$

$$\mathcal{V}^{(2)}\tau_n^{z}\mathcal{V}^{(2)\dagger} = -(P_m^{+} - P_m^{-})\tau_n^{z}, \tag{A2}$$

$$\mathcal{V}^{(2)}U_{mn}\mathcal{V}^{(2)\dagger} = \tau_m^{x}U_{mn}\tau_m^{x}. \tag{A3}$$

Acting with $\mathcal{V}^{(2)}$ on the Hamiltonian, we find that the electric part is invariant,

$$H_{\mathrm{E}}^{(2)} = \mathcal{V}^{(2)}H_{\mathrm{E}}^{(1)}\mathcal{V}^{(2)\dagger} = H_{\mathrm{E}}^{(1)} = \lambda_E \sum_{l=\mathrm{links}} |2, mn\rangle \langle 2, mn| . \tag{A4}$$

Recalling that Π ($\equiv \theta_{a^2}$) is defined as the difference between the $j = 2$ irrep projector and that for all the unfaithful irreps, we have

$$\Pi = \Pi_1 - \Pi_2 \quad H_{\mathrm{E}} = \lambda_E \sum_{l=\mathrm{links}} \Pi_{2,l}. \tag{A5}$$

By omitting constant terms and rearranging, we ultimately obtain a term expressed solely in Π, whose corresponding

gate form is known to be implementable [59],

$$H_{\mathrm{E}}^{(2)} = -\frac{\lambda_E}{2} \sum_{l=\text{links}} \Pi_l. \tag{A6}$$

Similarly to H_E, H_M is also invariant. Nevertheless, we take a step back and consider its effective form. From the Gauss's laws in Eq. (35), we can write the mass term using solely gauge fields,

$$H_{\mathrm{M}}^{(2)} = M \sum_{x,i} \varepsilon(\mathbf{x}) n_i(\mathbf{x}) = -\frac{M}{2} \sum_{x,i} W_i(\mathbf{x}). \tag{A7}$$

Recall that the $W_i(x)$, Eq. (16), consist of the operators θ_0 and θ_1, which again can be easily translated into gates (25).

The magnetic term H_B remains invariant, as it is a pure gauge contribution. Its form is identical to that presented in Eq. (29). Therefore, H_B involves only the gates corresponding to Π and U_{mn}.

Last, we examine the transformation of the interaction part,

$$H_{\mathrm{GM}}^{(2)} = \mathcal{V}^{(2)} H_{\mathrm{GM}}^{(1)} \mathcal{V}^{(2)\dagger}. \tag{A8}$$

Here we need how terms like $\tau_m^+(\mathbf{x}) U_{mn}(\mathbf{x}, 1) \tau_n^-(\mathbf{x} + \hat{\mathbf{e}}_1)$ are transformed under $\mathcal{V}^{(2)}$, resulting in [using Eq. (A1)]

$$(P_m^+ \sigma_m^- + P_m^- \sigma_m^+) \tau_m^+(\mathbf{x}) U_{mn}(\mathbf{x}) \tau_n^-(\mathbf{x} + e_1) (P_n^+ \sigma_n^+ + P_n^- \sigma_n^-). \tag{A9}$$

Reordering and using the properties of the τ-Pauli matrices, we observe that $H^{(2)}$ is block-diagonal in the matter spins, with static ($\tau_z = -1$) configurations. Using the constraints in Eq. (44), we can restrict ourselves to physical states by integrating out all the matter-down states. Formally, Eq. (44) implies that

$$|\psi^{(2)}\rangle = |\tilde{\psi}^{(2)}\rangle \otimes |\Omega\rangle, \tag{A10}$$

where $|\Omega\rangle$ is a product state of all matter spins pointing down, and $|\tilde{\psi}^{(2)}\rangle$ is a state of the gauge fields. Then we can define a Hamiltonian acting only on the gauge fields degrees of freedom via

$$\tilde{H}^{(2)} = \langle \Omega | H^{(2)} | \Omega \rangle, \tag{A11}$$

including $\tilde{H}_{\mathrm{M}}^{(2)} = H_{\mathrm{M}}^{(2)}$, $\tilde{H}_{\mathrm{E}}^{(2)} = H_{\mathrm{E}}^{(2)}$, and $\tilde{H}_{\mathrm{GM}}^{(2)}$.

The complete form of the final Hamiltonian becomes rather complicated. An explicit example is given in Sec. V. Assuming J is real-valued (which can be done without loss of generality for $d = 1$), the expression can be simplified by focusing exclusively on the anti-Hermitian components in the summation [like in (61)]. As shown in Fig. 10, the radius of interactions is extended after the transformations $\mathcal{V}^{(2)}$ and $\mathcal{V}^{(1)}$, but, importantly, they nevertheless remain local.

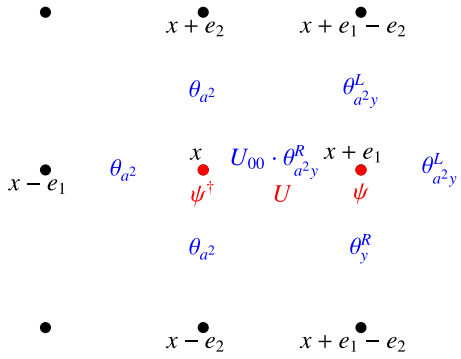

FIG. 10. Pictorial representation of an interaction term ($H^h_{00}(\mathbf{x})$). The vertices are empty as the matter fields have been eliminated. The blue operators act on the links (gauge d.o.f.); in red the original term.

APPENDIX B: ANALYTICAL VERIFICATION OF MATTER ELIMINATION IN TWO DIMENSIONS

1. The pseudo-2D system

In this appendix, we aim to verify the correctness of the transformations in the non-Abelian case and the resulting Hamiltonian. The most effective approach is to ensure that the spectrum of the Hamiltonian with matter aligns with that of the transformed one. While the primary objective of quantum simulation is to find spectra and states of complex systems, it is imperative to validate the model's accuracy. It may seem surprising that fermionic matter and the substantial redundancy can be addressed in this manner within a non-Abelian LGT. However, we demonstrate analytically that this approach is consistent and free of any irregularities.

Our strategy is as follows. First, we identify the gauge-invariant states and corresponding spectrum in the presence of matter. Next, we apply the transformations to these states and evaluate the spectrum. If the transformation is correct, the spectra must coincide. Subsequently, we derive the states from a pure gauge theory with the transformed constraints and verify that they match the original ones. Once this is established, we demonstrate that the transformations hold in the non-Abelian case.

a. Solution of the original model

We impose gauge invariance and determine the states satisfying the Gauss's laws. Drawing an analogy with the Wigner-Eckart theorem [69], we seek to ensure that, for each site, the combination of right irreps equals the sum of left irreps. This can be achieved by employing Clebsch-Gordan (CG) coefficients and subsequently verifying that the state maintains gauge invariance. The most general gauge-invariant state is given by (for the notation refer to Fig. 7)

$$\begin{aligned} |\Psi\rangle = \sum_{J_i, M_j, N_k} & \alpha^{J_1 J_2 J_3 j_a j_b j_c j_d}_{M_1 M_2 M_3 N_1 N_2 N_3} |J_1 M_1 N_1\rangle |J_2 M_2 N_2\rangle |J_3 M_3 N_3\rangle \\ & \times (a_0^\dagger)^{n_{a_0}} (a_1^\dagger)^{n_{a_1}} (b_0^\dagger)^{n_{b_0}} (b_1^\dagger)^{n_{b_1}} (c_0^\dagger)^{n_{c_0}} (c_1^\dagger)^{n_{c_1}} \\ & \times (d_0^\dagger)^{n_{d_0}} (d_1^\dagger)^{n_{d_1}} |\Omega\rangle, \end{aligned} \tag{B1}$$

where $|\Omega\rangle$ stands for the matter *Fock vacuum*. In addition, we impose the half-filling condition for the fermions.

By utilizing the Clebsch-Gordan coefficients detailed in Table II, we find a total of 10 gauge-invariant states, $\{|\Psi_i\rangle\}_{i=1,\ldots 10}$, for which we checked that they respect the different Gauss's laws. Moreover, we also assessed their rotational symmetry (under a rotation every state is mapped into another one) and verified that the Hamiltonian is rotationally invariant. The spectrum of the 10 states is given in Fig. 11.

TABLE II. Clebsch-Gordan coefficients, $m, m' \in \{0, 1\}$, computed using the Clebsch-Gordan series [103]: $D^{j_1}_{m_1 m_1'} D^{j_2}_{m_2 m_2'} = \sum_J \langle j_1 m_1 j_2 m_2 | JM \rangle \langle JM' | j_1 m_1' j_2 m_2' \rangle D^J_{MM'}$.

Coefficients				Value
$\langle 0\|00\rangle$,	$\langle 0\|\bar{0}\bar{0}\rangle$,	$\langle 0\|11\rangle$,	$\langle 0\|\bar{1}\bar{1}\rangle$	1
$\langle \bar{0}\|\bar{0}0\rangle$,	$\langle \bar{0}\|0\bar{0}\rangle$,	$\langle \bar{0}\|1\bar{1}\rangle$,	$\langle \bar{0}\|\bar{1}1\rangle$	1
$\langle 1\|10\rangle$,	$\langle 1\|01\rangle$,	$\langle 1\|\bar{0}\bar{1}\rangle$,	$\langle 1\|\bar{1}\bar{0}\rangle$	1
$\langle \bar{1}\|\bar{1}0\rangle$,	$\langle \bar{1}\|0\bar{1}\rangle$,	$\langle \bar{1}\|\bar{0}1\rangle$,	$\langle \bar{1}\|1\bar{0}\rangle$	1
$\langle 0, 2m\|2m'\rangle$,	$\langle 2m, 0\|2m'\rangle$			$\delta_{m,m'}$
$\langle \bar{0}, 2m\|2m'\rangle$,	$\langle 2m, \bar{0}\|2m'\rangle$			$\varepsilon_{m,m'}$
$\langle 1, 2m\|2m'\rangle$,	$\langle 2m, 1\|2m'\rangle$			$(\sigma_z)_{m,m'}$
$\langle \bar{1}, 2m\|2m'\rangle$,	$\langle 2m, \bar{1}\|2m'\rangle$			$(\sigma_x)_{m,m'}$
$\langle 0\|2m, 2m'\rangle$				$\frac{1}{\sqrt{2}}\delta_{m,m'}$
$\langle \bar{0}\|2m, 2m'\rangle$				$\frac{1}{\sqrt{2}}\epsilon_{m,m'}$
$\langle 1\|2m, 2m'\rangle$				$\frac{1}{\sqrt{2}}(\sigma_z)_{m,m'}$
$\langle \bar{1}\|2m, 2m'\rangle$				$\frac{1}{\sqrt{2}}(\sigma_x)_{m,m'}$

b. Solution of the transformed model

In the preceding section, we have identified the 10 gauge-invariant states, evaluated the Hamiltonian upon them, and plotted the resulting spectrum. Now we aim to determine the spectrum of the pseudo-2D model in the absence of matter and contrast it with the original one. We apply $\mathcal{V}^{(2)}$ [Eq. (42)] to the Hamiltonian and to the gauge-invariant states found before. For the Hamiltonian, the process is similar to the 2D analysis; see Appendix A for more details. In order to validate the transformed Hamiltonian, we proceed to compute the gauge-invariant states under $\mathcal{V}^{(2)}$. This computation allows us to compare the resulting spectrum with the analysis that includes the matter (Fig. 11). Moreover, from the explicit calculation we found that, as expected, the states $\{|\psi_i^{(2)}\rangle\}_{i=1,2...10}$ are simply deprived of the matter part, while the gauge fields remain unchanged.

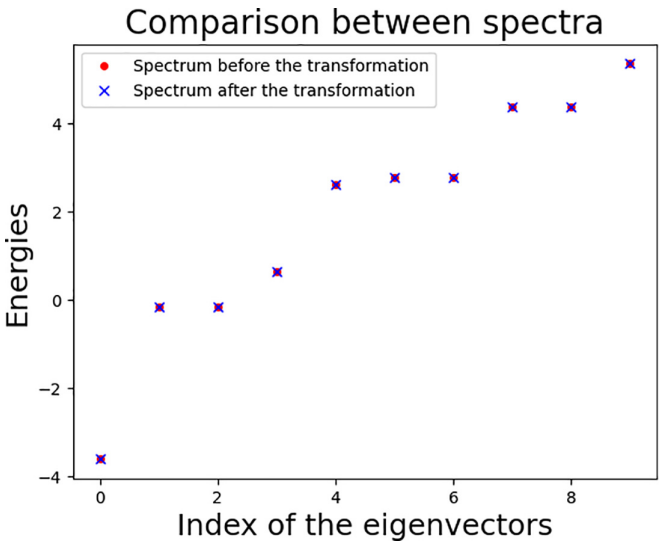

FIG. 11. Spectrum evaluated with $M = 1$, $\lambda_E = 1$, and $J = 1$. The solutions of the original and transformed model yield the same result, confirming the validity of the employed transformations.

c. Solution of a pure gauge theory

It is essential to verify that the 10 states are exhaustive. To achieve this, we begin with a pure-gauge theory and impose Gauss's laws. Since matter is no longer present, we must derive a new version of the Gauss's laws, which we achieve by applying $\mathcal{V}^{(2)}$ to Eq. (19):

$$W_g^{(2)}(\mathbf{x})\theta^{\dagger(2)}_{g,\mathrm{M}}(\mathbf{x})|\psi^{(2)}\rangle = |\psi^{(2)}\rangle \quad \forall \mathbf{x} \in \mathbb{Z}^d, \forall g \in \mathbb{D}_8. \tag{B2}$$

The most general state of a pure gauge theory is given by

$$|\psi^{(2)}\rangle = \sum_{J_i, M_j, N_l} \alpha^{J_1 J_2 J_3 j_a j_b j_c j_d}_{M_1 M_2 M_3 N_1 N_2 N_3} |J_1 M_1 N_1\rangle |J_2 M_2 N_2\rangle |J_3 M_3 N_3\rangle. \tag{B3}$$

We can substitute this state parametrization into Eq. (B2), where the solutions correspond to the states with eigenvalue 1. The desired states are determined by the intersection of the solutions derived from the various Gauss's laws. As a result, we obtain the same 10 states identified in Appendix B 1 b, thereby concluding the proof. In conclusion, the evidence of the pseudo-2D analysis validates both the transformation and the Hamiltonian.

2. The single-plaquette system

In this case, constructing the gauge-invariant states for a single plaquette (Fig. 12) as we did above in the case of the pseudo-2D model is significantly more involved. There are 158 of them and finding the explicit form analytically is not feasible. Nevertheless, we can use the above certification of the 2D model without plaquette term. The Hamiltonian of the plaquette can be extracted from the general 2D formulation as a particular case with known boundary conditions. In this case, we also take into account the magnetic term, which we have verified to be correct as

$$[W_g(\mathbf{x})\theta^{\dagger}_{g,M}(\mathbf{x}), H_B] = 0, \tag{B4}$$

$$[H_\mathrm{E}, H_\mathrm{B}] = 0 = [H_\mathrm{M}, H_\mathrm{B}] = 0 = [H_\mathrm{GM}, H_\mathrm{B}]. \tag{B5}$$

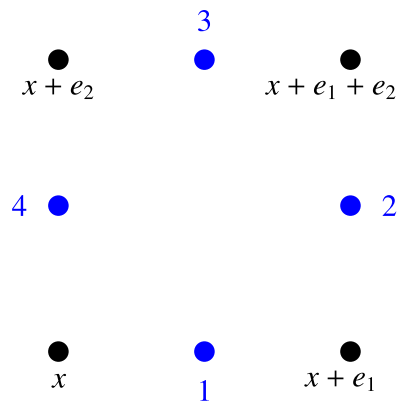

FIG. 12. Single plaquette, in blue the gauge field and in black the matter before being removed. x and $x + e_1 + e_2$ are taken as the even sites while $x + e_1$ and $x + e_2$ as the odd ones. Per site, we have at most two fermions corresponding to two different flavours. We defined the gauge Hilbert space as the product space of the links (1, 2, 3, and 4).

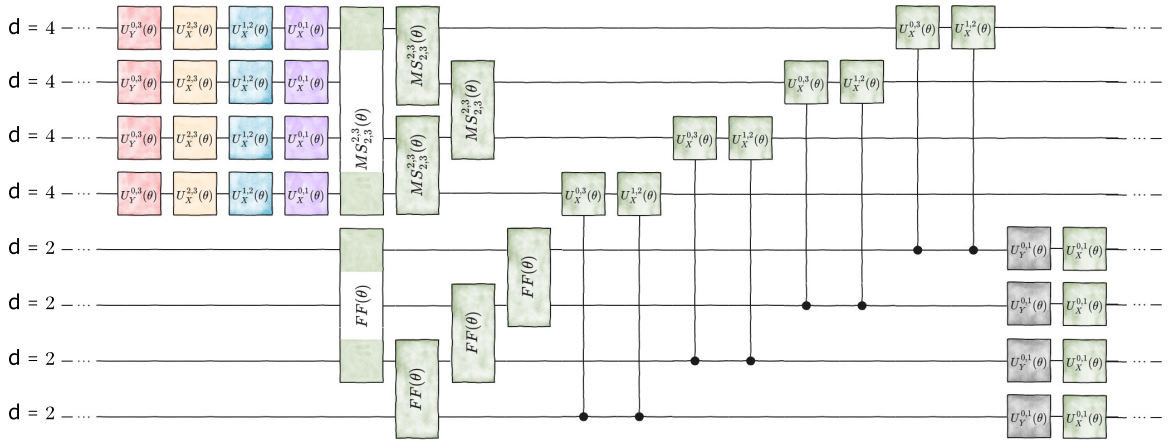

FIG. 13. Individual layer of the parametrized quantum circuit for ground state preparation of the plaquette system. Each layer of the parametrized quantum circuit used to find the approximate ground state of the plaquette system in 2D with non-Abelian $\mathbb{D}_8$-symmetry consists of two-level single-qudit rotations on the ququarts, entangling two-body MS gates between each pair of ququarts, entangling flip-flop gates between each pair of qubits, qubit-ququart controlled-rotation gates, and single-qubit Pauli-X and Pauli-Y rotations. Each gate in the variational circuit is parametrized by a variational parameter θ, which differs between different layers. Note that, in accordance with the convention used in the drawing software [94], the circuit is to be read from right to left.

By leveraging certain properties (Us and Π are Hermitian and real) derived from the gate formulation in Eq. (26), the magnetic term can be rewritten as a sum of 16 terms,

$$H_{\mathrm{B}} = 2Re[\lambda_b] \sum_{m,n,n',m'=0,1} \Pi^1 U^1_{mn} \Pi^2 U^2_{nn'} U^3_{m'n'} U^4_{mm'}. \quad \text{(B6)}$$

The theory developed for a single plaquette, while simple, presents significant interest for implementation on real quantum hardware. Indeed, it describes the smallest nontrivial system that is already challenging to treat both analytically and computationally, thus offering a valuable testbed for benchmarking practical quantum-computing and -simulation algorithms.

APPENDIX C: VARQITE FOR THE SINGLE-PLAQUETTE SYSTEM

Here we provide numerical simulations for the ground-state preparation of the single-plaquette system.

We employ the VarQITE algorithm for ground-state prepatation of the plaquette system for a set of coefficients in the Hamiltonian $J = M = h = 1$ and for the magnetic field coefficient $\lambda_b = 0.3$. As we show in the following, this point of the phase diagram is already characterized by a signicifant amount of entanglement. Therefore, designing a variational circuit with that is capable in capturing this complicated entanglement structure is challenging. Instead, we show how variational circuits on the edge of the experimental feasibility perform in preparing the ground state of the plaquette model.

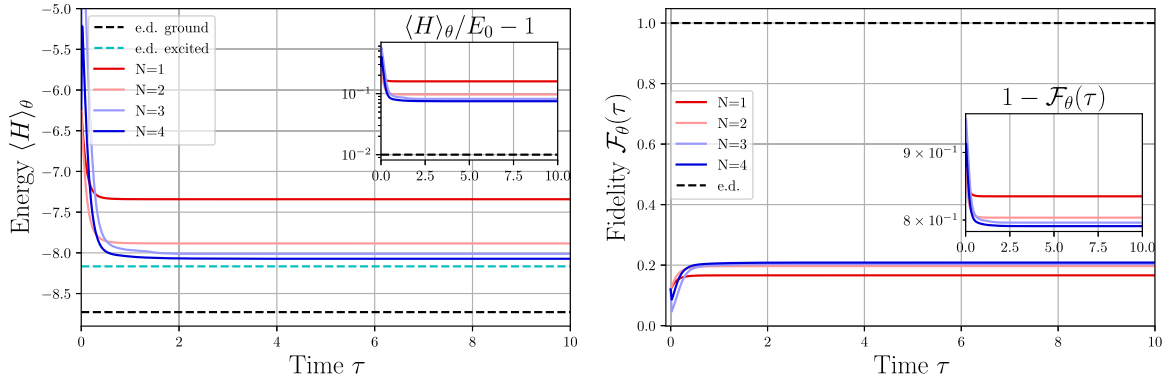

FIG. 14. VarQITE for the single-plaquette system: (a) The energy of the variational state $|\psi(\boldsymbol{\theta})\rangle$ as a function of the imaginary time for $N = 1, 2, 3, 4$ number of layers. The dashed black line shows the numerical value of the true ground state, whereas the cyan line of the numerical value of the gauge-invariant first excited state (here, in contrast to the 1D and the pseudo-2D cases, a small λ is sufficient to penalize the non-gauge-invariant states significantly and lift them above the gauge-invariant first excited state). The optimized state converges to some superposition of the ground state with the first few excited states and the difference between variational energy and the ground state energy does not drop below the gap. (b) The fidelity of the variational state w.r.t. the true ground state from exact diagonalization is shown as a function of the imaginary time τ. Although some improvement is visible, the fidelity does not reach above 90%.

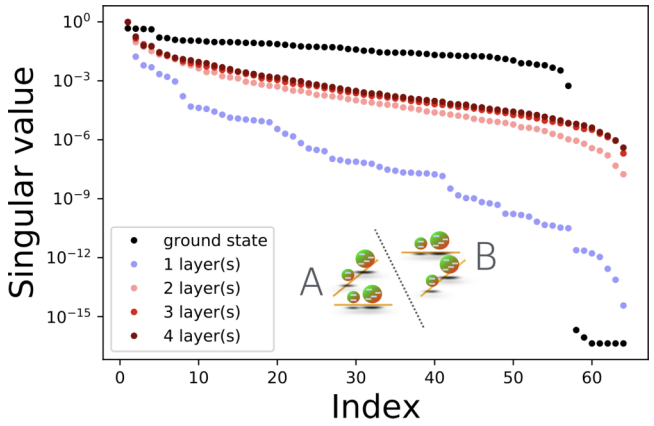

FIG. 15. Singular value decomposition of the reduced density matrix of subsystem A in the exact ground state (black dots) and in the optimized variational states for $N = 1, 2, 3, 4$ layers.

In other words, it is in general impossible to provide a rigorous estimate for the number, or order of magnitude, of entangling gates required in a variational circuit for the approximation of a quantum state with error ϵ. This is due to the fact that the variational approach is heuristic and works on the principle of trial and error. However, one can very much answer the opposite and much more experimentally relevant question: given a fixed finite amount of entangling gates, how well one can approximate a given quantum state (provided that one can estimate the fidelity between the variational approximation and this quantum state). This is what we address below.

The circuit we employ is shown in Fig. 13. The entangling operations in the circuit are the usual Mølmer-Sørensen gates between qudits, as well as the qubit-qubit flip-flop (FF) gate, given by

$$\mathrm{FF}(\theta) = \exp[-i\theta(\sigma^+ \otimes \sigma^- + \sigma^- \otimes \sigma^+)] \tag{C1}$$

and the qubit-qudit controlled-rotation (CROT) gate given by

$$\mathrm{CROT}_{k,ij}(\theta) = (\mathbf{1} - |k\rangle\langle k|) \otimes \mathbf{1} + |k\rangle\langle k| \otimes \exp\left(-i\theta\sigma_X^{i,j}\right). \tag{C2}$$

The flip-flop gate can be implemented by using one MS gate and single-qubit rotations and the CROT is a native gate on the trapped-ion qudit device [28]. Each gate is parametrized by a variational parameter. We initialize the system in the product state $|\psi_0\rangle = \frac{1}{N_0}\bigotimes_{i=1}^{4}\sum_{\alpha=0}^{1}|\alpha\rangle_{b,i} \otimes \sum_{\beta=0}^{3}|\beta\rangle_{d,i}$, which can be easily prepared on the trapped-ion quantum computer by applying a sequence of single-qudit operations, such as Hadamard and generalized Hadamard gates, on a computational basis state. Here $N_0 = 8^2$ is a normalization factor. At each time step of the minimization, we measure the energy of the plaquette system in the variational state $E(\boldsymbol{\theta}) = \langle\psi(\boldsymbol{\theta})|H|\psi(\boldsymbol{\theta})\rangle$ and the fidelity w.r.t. the exactly diagonalized ground state $|\psi_{\mathrm{ground}}\rangle$. Here, as in the other cases, we add to the Hamiltonian the penalty term $H \to H + \lambda\sum_i G_i^2$, where G_i is the Gauss's law operator at site i and λ is a Lagrange multiplier. We have chosen $\lambda = 0.1$ for numerical stability. The results of the optimization procedure are shown in Fig. 14.

In order to evaluate possible reasons for why the variational circuit is not able to deliver a high-fidelity approximation of the ground state, we look at the entangling structure of the ground state and additionally, of the converged variational state for $N = 1, 2, 3$ and 4 layers. Specifically, we perform singular value decomposition (SVD) of the reduced density matrix of subsystem A (see Fig. 15) for the variational states and for the exact ground state. We observe that, with the increase of the number of layers, the entangling structure of the optimized variational state is only slightly changing, where there is almost no difference between three and four layers. Therefore, we conclude that, even though the circuit could, in principle, capture the entangling structure of the ground state already for a modest gate count, in practice the algorithm converges to a state that is not the true ground state, but just a local minimum. While a proper study of how to devise the variational circuit for obtaining a high-fidelity approximation of the ground state of the plaquette goes beyond the scope of this work, we believe that the bottleneck for the optimization is on the side of the optimizer strategy and not on the gate count. Perhaps more sophisticated variational algorithms [84,104] and tailoring the cost function in some way will provide a viable way towards high fidelities.

[1] C. Quigg, The quantum theory of fields, Science **275**, 938 (1997).
[2] J. D. Bjorken, Asymptotic sum rules at infinite momentum, Phys. Rev. **179**, 1547 (1969).
[3] D. Gross and F. Wilczek, Ultraviolet behavior of non-Abelian gauge theories, Phys. Rev. Lett. **30**, 1343 (1973).
[4] K. Wilson, Confinement of quarks, Phys. Rev. D **10**, 2445 (1974).
[5] J. Kogut and L. Susskind, Hamiltonian formulation of Wilson's lattice gauge theories, Phys. Rev. D **11**, 395 (1975).
[6] J. Kogut, An introduction to lattice gauge theory and spin systems, Rev. Mod. Phys. **51**, 659 (1979).
[7] M. Troyer and U.-J. Wiese, Computational complexity and fundamental limitations to fermionic quantum Monte Carlo simulations, Phys. Rev. Lett. **94**, 170201 (2005).
[8] R. Feynman, Simulating physics with computers, Int. J. Theor. Phys. **21**, 467 (1982).
[9] U.-J. Wiese, Ultracold quantum gases and lattice systems: Quantum simulation of lattice gauge theories, Ann. Phys. **525**, 777 (2013).
[10] E. Zohar, J. Cirac, and B. Reznik, Quantum simulations of lattice gauge theories using ultracold atoms in optical lattices, Rep. Prog. Phys. **79**, 014401 (2016).
[11] U.-J. Wiese, Towards quantum simulating QCD, Nucl. Phys. A **931**, 246 (2014).
[12] M. Dalmonte and S. Montangero, Lattice gauge theory simulations in the quantum information era, Contemp. Phys. **57**, 388 (2016).
[13] M. C. Bañuls and K. Cichy, Review on novel methods for lattice gauge theories, Rep. Prog. Phys. **83**, 024401 (2020).
[14] M. C. Bañuls, R. Blatt, J. Catani, A. Celi, J. I. Cirac, M. Dalmonte, L. Fallani, K. Jansen, M. Lewenstein, S. Montangero *et al.*, Simulating lattice gauge theories within quantum technologies, Eur. Phys. J. D **74**, 165 (2020).

[15] N. Klco, A. Roggero, and M. Savage, Standard model physics and the digital quantum revolution: Thoughts about the interface, Rep. Prog. Phys. **85**, 064301 (2022).
[16] E. Zohar, Quantum simulation of lattice gauge theories in more than one space dimension—Requirements, challenges, methods, Philos. Trans. R. Soc. A **380**, 20210069 (2022).
[17] M. Aidelsburger, L. Barbiero, A. Bermudez, T. Chanda, A. Dauphin, D. González-Cuadra, P. R. Grzybowski, S. Hands, F. Jendrzejewski, J. Jünemann *et al.*, Cold atoms meet lattice gauge theory, Philos. Trans. R. Soc. A **380**, 20210064 (2022).
[18] A. Di Meglio, K. Jansen, I. Tavernelli, C. Alexandrou, S. Arunachalam, C. W. Bauer, K. Borras, S. Carrazza, A. Crippa, V. Croft *et al.*, Quantum computing for high-energy physics: State of the art and challenges, PRX Quantum **5**, 037001 (2024).
[19] J. C. Halimeh, M. Aidelsburger, F. Grusdt, P. Hauke, and B. Yang, Cold-atom quantum simulators of gauge theories, Nat. Phys. **21**, 25 (2025).
[20] C. Schweizer, F. Grusdt, M. Berngruber, L. Barbiero, E. Demler, N. Goldman, I. Bloch, and M. Aidelsburger, Floquet approach to $\mathbb{Z}_2$ lattice gauge theories with ultracold atoms in optical lattices, Nat. Phys. **15**, 1168 (2019).
[21] A. Mil, T. V. Zache, A. Hegde, A. Xia, R. P. Bhatt, M. K. Oberthaler, P. Hauke, J. Berges, and F. Jendrzejewski, A scalable realization of local U(1) gauge invariance in cold atomic mixtures, Science **367**, 1128 (2020).
[22] B. Yang, H. Sun, R. Ott, H.-Y. Wang, T. V. Zache, J. C. Halimeh, Z.-S. Yuan, P. Hauke, and J.-W. Pan, Observation of gauge invariance in a 71-site Bose-Hubbard quantum simulator, Nature (London) **587**, 392 (2020).
[23] Z.-Y. Zhou, G.-X. Su, J. C. Halimeh, R. Ott, H. Sun, P. Hauke, B. Yang, Z.-S. Yuan, J. Berges, and J.-W. Pan, Thermalization dynamics of a gauge theory on a quantum simulator, Science **377**, 311 (2022).
[24] D. Gonzalez-Cuadra, M. Hamdan, T. V. Zache, B. Braverman, M. Kornjaca, A. Lukin, S. H. Cantu, F. Liu, S.-T. Wang, A. Keesling *et al.*, Observation of string breaking on a (2 + 1)D Rydberg quantum simulator, Nature (London) **642**, 321 (2025).
[25] E. A. Martinez, C. A. Muschik, P. Schindler, D. Nigg, A. Erhard, M. Heyl, P. Hauke, M. Dalmonte, T. Monz, P. Zoller, and R. Blatt, Real-time dynamics of lattice gauge theories with a few-qubit quantum computer, Nature (London) **534**, 516 (2016).
[26] C. Kokail, C. Maier, R. van Bijnen, T. Brydges, M. K. Joshi, P. Jurcevic, C. A. Muschik, P. Silvi, R. Blatt, C. F. Roos, and P. Zoller, Self-verifying variational quantum simulation of lattice models, Nature (London) **569**, 355 (2019).
[27] N. H. Nguyen, M. C. Tran, Y. Zhu, A. M. Green, C. H. Alderete, Z. Davoudi, and N. M. Linke, Digital quantum simulation of the Schwinger model and symmetry protection with trapped ions, PRX Quantum **3**, 020324 (2022).
[28] M. Meth, J. F. Haase, J. Zhang, C. Edmunds, L. Postler, A. Steiner, A. J. Jena, L. Dellantonio, R. Blatt, P. Zoller *et al.*, Simulating 2D lattice gauge theories on a qudit quantum computer, Nat. Phys. **21**, 570 (2025).
[29] A. Mezzacapo, E. Rico, C. Sabín, I. L. Egusquiza, L. Lamata, and E. Solano, Non-Abelian SU(2) lattice gauge theories in superconducting circuits, Phys. Rev. Lett. **115**, 240502 (2015).
[30] N. Klco, E. F. Dumitrescu, A. J. McCaskey, T. D. Morris, R. C. Pooser, M. Sanz, E. Solano, P. Lougovski, and M. J. Savage, Quantum-classical computation of Schwinger model dynamics using quantum computers, Phys. Rev. A **98**, 032331 (2018).
[31] Y. Y. Atas, J. Zhang, R. Lewis, A. Jahanpour, J. F. Haase, and C. A. Muschik, SU(2) hadrons on a quantum computer via a variational approach, Nat. Commun. **12**, 6499 (2021).
[32] J. Mildenberger, W. Mruczkiewicz, J. C. Halimeh, Z. Jiang, and P. Hauke, Confinement in a $\mathbb{Z}_2$ lattice gauge theory on a quantum computer, Nat. Phys. **21**, 312 (2025).
[33] E. Zohar and J. Cirac, Eliminating fermionic matter fields in lattice gauge theories, Phys. Rev. B **98**, 075119 (2018).
[34] E. Zohar and J. Cirac, Removing staggered fermionic matter in U(N) and SU(N) lattice gauge theories, Phys. Rev. D **99**, 114511 (2019).
[35] G. Pardo, T. Greenberg, A. Fortinsky, N. Katz, and E. Zohar, Resource-efficient quantum simulation of lattice gauge theories in arbitrary dimensions: Solving for Gauss's law and fermion elimination, Phys. Rev. Res. **5**, 023077 (2023).
[36] R. Irmejs, M.-C. Bañuls, and J. I. Cirac, Quantum simulation of $\mathbb{Z}_2$ lattice gauge theory with minimal resources, Phys. Rev. D **108**, 074503 (2023).
[37] P. Jordan and E. Wigner, Über das Paulische Äquivalenzverbot, Z. Phys. **47**, 631 (1928).
[38] H. Lamm, S. Lawrence, and Y. Yamauchi (NuQS Collaboration), General methods for digital quantum simulation of gauge theories, Phys. Rev. D **100**, 034518 (2019).
[39] M. S. Alam, S. Hadfield, H. Lamm, and A. C. Y. Li (SQMS Collaboration), Primitive quantum gates for dihedral gauge theories, Phys. Rev. D **105**, 114501 (2022).
[40] D. González-Cuadra, T. V. Zache, J. Carrasco, B. Kraus, and P. Zoller, Hardware efficient quantum simulation of non-Abelian gauge theories with qudits on Rydberg platforms, Phys. Rev. Lett. **129**, 160501 (2022).
[41] E. Ballini, J. Mildenberger, M. M. Wauters, and P. Hauke, Symmetry verification for noisy quantum simulations of non-Abelian lattice gauge theories, arXiv:2412.07844 (2024).
[42] S. Notarnicola, E. Ercolessi, P. Facchi, G. Marmo, S. Pascazio, and F. V. Pepe, Discrete Abelian gauge theories for quantum simulations of QED, J. Phys. A: Math. Theor. **48**, 30FT01 (2015).
[43] E. Zohar, A. Farace, B. Reznik, and J. Cirac, Digital lattice gauge theories, Phys. Rev. A **95**, 023604 (2017).
[44] E. Zohar, A. Farace, B. Reznik, and J. I. Cirac, Digital quantum simulation of $\mathbb{Z}_2$ Lattice Gauge Theories with Dynamical Fermionic Matter, Phys. Rev. Lett. **118**, 070501 (2017).
[45] E. Ercolessi, P. Facchi, G. Magnifico, S. Pascazio, and F. V. Pepe, Phase transitions in Z_n gauge models: Towards quantum simulations of the schwinger-weyl qed, Phys. Rev. D **98**, 074503 (2018).
[46] J. Bender, E. Zohar, A. Farace, and J. Cirac, Digital quantum simulation of lattice gauge theories in three spatial dimensions, New J. Phys. **20**, 093001 (2018).
[47] L. Barbiero, C. Schweizer, M. Aidelsburger, E. Demler, N. Goldman, and F. Grusdt, Coupling ultracold matter to dynamical gauge fields in optical lattices: From flux attachment to $\mathbb{Z}_2$ lattice gauge theories, Sci. Adv. **5**, eaav7444 (2019).
[48] D. González-Cuadra, L. Tagliacozzo, M. Lewenstein, and A. Bermudez, Robust topological order in fermionic $\mathbb{Z}_2$ gauge

theories: From Aharonov-Bohm instability to soliton-induced deconfinement, Phys. Rev. X **10**, 041007 (2020).

[49] L. Homeier, C. Schweizer, M. Aidelsburger, A. Fedorov, and F. Grusdt, $\mathbb{Z}_2$ lattice gauge theories and Kitaev's toric code: A scheme for analog quantum simulation, Phys. Rev. B **104**, 085138 (2021).

[50] E. J. Gustafson and H. Lamm, Toward quantum simulations of $\mathbb{Z}_2$ gauge theory without state preparation, Phys. Rev. D **103**, 054507 (2021).

[51] L. Lumia, P. Torta, G. B. Mbeng, G. E. Santoro, E. Ercolessi, M. Burrello, and M. M. Wauters, Two-dimensional $\mathbb{Z}_2$ lattice gauge theory on a near-term quantum simulator: Variational quantum optimization, confinement, and topological order, PRX Quantum **3**, 020320 (2022).

[52] R. Samajdar, D. G. Joshi, Y. Teng, and S. Sachdev, Emergent $\mathbb{Z}_2$ gauge theories and topological excitations in Rydberg atom arrays, Phys. Rev. Lett. **130**, 043601 (2023).

[53] E. J. Gustafson, H. Lamm, F. Lovelace, and D. Musk, Primitive quantum gates for an SU(2) discrete subgroup: Binary tetrahedral, Phys. Rev. D **106**, 114501 (2022).

[54] E. J. Gustafson, Y. Ji, H. Lamm, E. M. Murairi, S. O. Perez, and S. Zhu, Primitive quantum gates for an $SU(3)$ discrete subgroup: $\Sigma(36 \times 3)$, Phys. Rev. D **110**, 034515 (2024).

[55] E. J. Gustafson, H. Lamm, and F. Lovelace, Primitive quantum gates for an $SU(2)$ discrete subgroup: Binary octahedral, Phys. Rev. D **109**, 054503 (2024).

[56] H. Lamm, Y.-Y. Li, J. Shu, Y.-L. Wang, and B. Xu, Block encodings of discrete subgroups on a quantum computer, Phys. Rev. D **110**, 054505 (2024).

[57] L. Homeier, A. Bohrdt, S. Linsel, E. Demler, J. C. Halimeh, and F. Grusdt, Realistic scheme for quantum simulation of $\mathbb{Z}_2$ lattice gauge theories with dynamical matter in $(2 + 1)$D, Commun. Phys. **6**, 127 (2023).

[58] A. Mariani, S. Pradhan, and E. Ercolessi, Hamiltonians and gauge-invariant Hilbert space for lattice Yang-Mills-like theories with finite gauge group, Phys. Rev. D **107**, 114513 (2023).

[59] M. Ringbauer, M. Meth, L. Postler, R. Stricker, R. Blatt, P. Schindler, and T. Monz, A universal qudit quantum processor with trapped ions, Nat. Phys. **18**, 1053 (2022).

[60] P. P. Popov, M. Meth, M. Lewestein, P. Hauke, M. Ringbauer, E. Zohar, and V. Kasper, Variational quantum simulation of U(1) lattice gauge theories with qudit systems, Phys. Rev. Res. **6**, 013202 (2024).

[61] G. Calajó, G. Magnifico, C. Edmunds, M. Ringbauer, S. Montangero, and P. Silvi, Digital quantum simulation of a (1+1)D SU(2) lattice gauge theory with ion qudits, PRX Quantum **5**, 040309 (2024).

[62] M. Illa, C. E. P. Robin, and M. J. Savage, Qu8its for quantum simulations of lattice quantum chromodynamics, Phys. Rev. D **110**, 014507 (2024).

[63] T. V. Zache, D. González-Cuadra, and P. Zoller, Fermion-qudit quantum processors for simulating lattice gauge theories with matter, Quantum **7**, 1140 (2023).

[64] N. Tantivasadakarn, R. Verresen, and A. Vishwanath, Shortest route to non-Abelian topological order on a quantum processor, Phys. Rev. Lett. **131**, 060405 (2023).

[65] M. Iqbal, N. Tantivasadakarn, R. Verresen, S. L. Campbell, J. M. Dreiling, C. Figgatt, J. P. Gaebler, J. Johansen, M. Mills, S. A. Moses *et al.*, Non-Abelian topological order and anyons on a trapped-ion processor, Nature (London) **626**, 505 (2024).

[66] L. Byles, E. Forbes, and J. K. Pachos, Demonstrating anyonic non-Abelian statistics with a minimal $d = 6$ qudit lattice, arXiv:2408.03377.

[67] D. Horn, M. Weinstein, and S. Yankielowicz, Hamiltonian approach to $Z(N)$ lattice gauge theories, Phys. Rev. D **19**, 3715 (1979).

[68] V. Kasper, G. Juzeliūnas, M. Lewenstein, F. Jendrzejewski, and E. Zohar, From the Jaynes–Cummings model to non-Abelian gauge theories: A guided tour for the quantum engineer, New J. Phys. **22**, 103027 (2020).

[69] E. Wigner, *Group Theory: And Its Application to the Quantum Mechanics of Atomic Spectra*, Pure and Applied Physics (Elsevier, New-York, 2012), Vol. 5.

[70] E. Zohar and M. Burrello, Formulation of lattice gauge theories for quantum simulations, Phys. Rev. D **91**, 054506 (2015).

[71] L. Susskind, Lattice fermions, Phys. Rev. D **16**, 3031 (1977).

[72] C. Hamer, Lattice model calculations for SU(2) Yang-Mills theory in $1 + 1$ dimensions, Nucl. Phys. B **121**, 159 (1977).

[73] M. C. Bañuls, K. Cichy, J. I. Cirac, K. Jansen, and S. Kühn, Efficient basis formulation for $(1 + 1)$-dimensional SU(2) lattice gauge theory: Spectral calculations with matrix product states, Phys. Rev. X **7**, 041046 (2017).

[74] P. Sala, T. Shi, S. Kühn, M. C. Bañuls, E. Demler, and J. I. Cirac, Variational study of U(1) and SU(2) lattice gauge theories with Gaussian states in $1 + 1$ dimensions, Phys. Rev. D **98**, 034505 (2018).

[75] M. Cerezo, A. Arrasmith, R. Babbush, S. C. Benjamin, S. Endo, K. Fujii, J. R. McClean, K. Mitarai, X. Yuan, L. Cincio, and P. J. Coles, Variational quantum algorithms, Nat. Rev. Phys. **3**, 625 (2021).

[76] K. Ito, W. Mizukami, and K. Fujii, Universal noise-precision relations in variational quantum algorithms, Phys. Rev. Res. **5**, 023025 (2023).

[77] T. Hoefler, T. Häner, and M. Troyer, Disentangling hype from practicality: On realistically achieving quantum advantage, Commun. ACM **66**, 82 (2023).

[78] J. R. McClean, S. Boixo, V. N. Smelyanskiy, R. Babbush, and H. Neven, Barren plateaus in quantum neural network training landscapes, Nat. Commun. **9**, 4812 (2018).

[79] R. R. Ferguson, L. Dellantonio, A. A. Balushi, K. Jansen, W. Dür, and C. A. Muschik, Measurement-based variational quantum eigensolver, Phys. Rev. Lett. **126**, 220501 (2021).

[80] D. Paulson, L. Dellantonio, J. F. Haase, A. Celi, A. Kan, A. Jena, C. Kokail, R. van Bijnen, K. Jansen, P. Zoller, and C. A. Muschik, Simulating 2D effects in lattice gauge theories on a quantum computer, PRX Quantum **2**, 030334 (2021).

[81] J. Zhang, R. Ferguson, S. Kühn, J. F. Haase, C. Wilson, K. Jansen, and C. A. Muschik, Simulating gauge theories with variational quantum eigensolvers in superconducting microwave cavities, Quantum **7**, 1148 (2023).

[82] A. Chan, Z. Shi, L. Dellantonio, W. Dür, and C. A. Muschik, Measurement-based infused circuits for variational quantum eigensolvers, Phys. Rev. Lett. **132**, 240601 (2024).

[83] R. C. Farrell, M. Illa, A. N. Ciavarella, and M. J. Savage, Quantum simulations of hadron dynamics in the Schwinger model using 112 qubits, Phys. Rev. D **109**, 114510 (2024).

[84] R. C. Farrell, M. Illa, A. N. Ciavarella, and M. J. Savage, Scalable circuits for preparing ground states on digital quantum computers: The Schwinger model vacuum on 100 qubits, PRX Quantum **5**, 020315 (2024).

[85] R. C. Farrell, M. Illa, and M. J. Savage, Steps toward quantum simulations of hadronization and energy loss in dense matter, Phys. Rev. C **111**, 015202 (2025).
[86] Y. Guo, T. Angelides, K. Jansen, and S. Kühn, Concurrent VQE for simulating excited states of the Schwinger model, arXiv:2407.15629.
[87] Y. Y. Atas, J. F. Haase, J. Zhang, V. Wei, S. M.-L. Pfaendler, R. Lewis, and C. A. Muschik, Simulating one-dimensional quantum chromodynamics on a quantum computer: Real-time evolutions of tetra- and pentaquarks, Phys. Rev. Res. **5**, 033184 (2023).
[88] X. Yuan, S. Endo, Q. Zhao, Y. Li, and S. C. Benjamin, Theory of variational quantum simulation, Quantum **3**, 191 (2019).
[89] B. Camino, J. Buckeridge, P. A. Warburton, V. Kendon, and S. M. Woodley, Quantum computing and materials science: A practical guide to applying quantum annealing to the configurational analysis of materials, J. Appl. Phys. **133**, 221102 (2023).
[90] J. D. Weidman, M. Sajjan, C. Mikolas, Z. J. Stewart, J. Pollanen, S. Kais, and A. K. Wilson, Quantum computing and chemistry, Cell Rep. Phys. Sci. **5**, 102105 (2024).
[91] M. Mörchen, G. H. Low, T. Weymuth, H. Liu, M. Troyer, and M. Reiher, Classification of electronic structures and state preparation for quantum computation of reaction chemistry, arXiv:2409.08910.
[92] W. van Dam, H. Liu, G. H. Low, A. Paetznick, A. Paz, M. Silva, A. Sundaram, K. Svore, and M. Troyer, End-to-end quantum simulation of a chemical system, arXiv:2409.05835.
[93] T. L. Scholten, C. J. Williams, D. Moody, M. Mosca, W. Hurley, W. J. Zeng, M. Troyer, and J. M. Gambetta, Assessing the benefits and risks of quantum computers, arXiv:2401.16317.
[94] J. Wilkens, Quantum circuit library (2023), https://github.com/wilkensJ/drawio-library.
[95] E. Zohar and J. Cirac, Combining tensor networks with Monte Carlo methods for lattice gauge theories, Phys. Rev. D **97**, 034510 (2018).
[96] A. Kelman, U. Borla, I. Gomelski, J. Elyovich, G. Roose, P. Emonts, and E. Zohar, Gauged Gaussian projected entangled pair states: A high dimensional tensor network formulation for lattice gauge theories, Phys. Rev. D **110**, 054511 (2024).
[97] J. Berges, What ultracold atoms tell us about the real-time dynamics of QCD in extreme conditions, EPJ Web Conf. **296**, 01021 (2024).
[98] R. Brower, S. Chandrasekharan, and U.-J. Wiese, QCD as a quantum link model, Phys. Rev. D **60**, 094502 (1999).
[99] C. W. Bauer and D. M. Grabowska, Efficient representation for simulating U(1) gauge theories on digital quantum computers at all values of the coupling, Phys. Rev. D **107**, L031503 (2023).
[100] D. M. Grabowska, C. F. Kane, and C. W. Bauer, A fully gauge-fixed SU(2) Hamiltonian for quantum simulations, Phys. Rev. D **111**, 114516 (2025).
[101] P. Fontana, M. M. Riaza, and A. Celi, An efficient finite-resource formulation of non-Abelian lattice gauge theories beyond one dimension, arXiv:2409.04441.
[102] E. Gaz, P. Popov, G. Pardo, M. Lewenstein, P. Hauke, and E. Zohar, Zenodo (2025), doi:10.5281/zenodo.15017288.
[103] D. M. Brink and G. R. Satchler, *Angular Momentum* (Oxford University Press, Oxford, 1994).
[104] N. Gomes, A. Mukherjee, F. Zhang, T. Iadecola, C. Wang, K. Ho, P. P. Orth, and Y. Yao, Adaptive variational quantum imaginary time evolution approach for ground state preparation, Adv. Quantum Technol. **4**, 2100114 (2021).